hydrogen

MDPI

Article

Bounding the Biohydrogen Potential of Organic Market Waste: Fruit-Fraction-Dependent Acidogenesis, Non-Additive Mixture Response, and Overestimation of Avoided-Methane Credits

Nicole Francisca Cabezas Alberto [1], Aleli Hanampa Valdivia [1], Yoisdel Castillo Alvarez [1,*] and Reinier Jiménez Borges [2,*]

[1] Environmental Engineering Career, Faculty of Engineering, Universidad Peruana de Ciencias Aplicadas (UPC), Lima 15023, Peru; u20211d977@upc.edu.pe (N.F.C.A.); u202120571@upc.edu.pe (A.H.V.)
[2] Department of Mechanical Engineering, Faculty of Engineering, Universidad de Cienfuegos "Carlos Rafael Rodríguez", Cienfuegos 59430, Cuba
* Correspondence: pcigycas@upc.edu.pe (Y.C.A.); rjimenezborges@gmail.com (R.J.B.)

Abstract

Dark fermentation of market waste is repeatedly proposed as a decentralized biohydrogen pathway for Latin American cities, and its climate benefit is almost invariably credited using the IPCC Tier-1 term for avoided methane applied to the full diverted mass. This study evaluates how much hydrogen this waste stream can actually deliver and whether such a credit survives a stoichiometric balance. A seven-day gravimetric survey of 10 stalls at El Pino Market (Carabayllo, Lima, Peru) yielded 754.6 kg week^{-1}, distributed as 41.04% fruit, 22.82% vegetables, and 36.14% cooked food.Four mixtures reproducing the recorded generation ratios of fruit (F), vegetables (V), and cooked food (A) were fermented in batch reactors in quintuplicate for 72 h: (F + V, V + A, F + A, and F + V + A). were fermented in batch reactors, with cumulative gas recorded every 6 h, yielding 240 observations. The modified Gompertz model fitted all curves ($R^2 = 0.982$–0.994). Specific yields were 26.45 mL g^{-1} VS for F + A, 18.89 for F + V, 18.41 for F + V + A, and only 0.63 for the fruit-free V + A mixture (Welch's ANOVA $F_{3,7.32} = 8.65 \times 10^4$, $p < 0.001$; Games–Howell separated all pairs except F + V versus F + V + A, $p = 0.713$). A linear Scheffé mixture model formulated on volatile-solids fractions and calibrated on the three fruit-containing mixtures predicted 5.48 mL g^{-1} VS for V + A, whereas the observed value was 11.6% of that prediction (95% bootstrap CI 9.8–13.7%), an 88.4% suppression of total fermentative gas that persists under every admissible additive null (2.5–13.7%) and cannot be explained by substrate concentration. Because the gas phase was not speciated, hydrogen production is bounded between an upper bound in which all gas is H_2 and a reference case was measured at 45% v/v, yielding 11.90–26.45 mL H_2 g^{-1} VS for the best-performing mixture. Even at the upper bound, stoichiometric closure relative to the acetate pathway reaches only 9.71%, and energy recovery amounts to 0.76–1.68% of the substrate chemical energy, compared with 73.8–84.3% for a methanogenic reference. A carbon and energy balance shows that more than 98% of the substrate energy and more than 95% of the carbohydrate carbon leave the process in the effluent. Acidogenesis therefore leaves most of the degradable organic carbon in the effluent, and the uncorrected Tier-1 credit of 29.44 t CO_2eq yr^{-1} overestimates the attainable benefit by a factor of 10 to 23 when scaled by the H_2-based stoichiometric proxy (1.29–2.86 t CO_2eq yr^{-1}), and by a factor of 15 to 69 when scaled by the pathway-consistent carbon-based factor (0.43–1.90 t CO_2eq yr^{-1}). The biohydrogen potential of market waste is therefore bounded by its fruit fraction; fruit-free mixtures are not merely poorer but fermentatively suppressed; and avoided-methane credits must be

Check for updates

Academic Editor: Silvano Tosti

Received: 16 August 2026
Revised: 10 September 2026
Accepted: 17 September 2026
Published: 24 September 2026

Copyright: © 2026 by the authors. Licensee MDPI, Basel, Switzerland. This article is an open access article distributed under the terms and conditions of the Creative Commons Attribution (CC BY) license.

constrained by measured process conversion and by the fate of residual carbon rather than by diverted waste mass alone.

Keywords: biohydrogen; dark fermentation; hydrogen from organic waste; stoichiometric closure; modified Gompertz kinetics; mixture design; avoided-methane accounting; circular bioeconomy

1. Introduction

Hydrogen produced by dark fermentation of organic waste occupies a distinctive position in the circular bioeconomy: it converts soluble carbohydrates within hours rather than weeks, does not require methanogenic acclimation, and produces an effluent rich in volatile fatty acids that can be subsequently valorized [1–3]. The focus of this study is a specific regime within this pathway, which should be defined from the outset: batch acidogenic fermentation at decentralized scale using market waste without additional segregation, without pH control during fermentation, or inoculum addition; that is, the configuration that can realistically be implemented in a Latin American municipal market. The Peruvian context makes this question particularly relevant: the organic fraction accounts for 57.2% of municipal solid waste, national waste generation increased from 6.90 to 8.71 million tonnes between 2014 and 2023, and approximately 1800 municipal dumpsites remain without gas capture [4,5]; the 24 most critical open dumpsites alone are projected to add 4.4 Mt CO_2eq between 2019 and 2028 [6].

The state of the art for this pathway can be organized around three axes. The first is thermodynamic and metabolic: the acetate pathway sets an upper yield of 4 mol H_2 per mol of hexose, while the butyrate pathway yields 2, meaning that every real reactor operates at some distance from a known theoretical ceiling [7,8]. The second is operational and ecological: pH, inoculum pretreatment, and microbial competition determine this distance, and contamination by lactic acid bacteria has in particular been identified as a central obstacle to scale-up, to the extent that lactate has shifted from being regarded primarily as an inhibitory sink to being considered a potentially recoverable intermediate [9–14]. The third is evaluative: two-stage schemes coupling dark fermentation and photofermentation offer the possibility of recovering residual potential [15,16], although photochemical efficiency and illumination design impose stringent constraints [17,18], while the climate benefit is commonly calculated using the default IPCC equation applied to the diverted waste mass [19,20].

Since 2022, the experimental literature has advanced rapidly in four directions that delimit the contribution of this work more precisely. First, pH, solids content, lactate availability, and substrate-specific optimization have been shown to redirect the metabolic spectrum of food-waste fermentation markedly [21–23]. Second, continuous systems have begun to resolve stability under load disturbances and to separate lactate production from H_2 production deliberately [24–26]. Third, waste mixing has been shown to alter not only substrate supply but also the interactions between H_2 producers and consumers [27,28]. Finally, pilot-scale and life-cycle studies have shifted the question from how much H_2 is produced to how much energy and net mitigation the system delivers [29–31]. However, no study among those reviewed simultaneously combines a mixture composition inherited from a real waste census, a formal non-additivity test against an excluded composition, a closure against the stoichiometric ceiling, and an explicit constraint of the climate benefit by the experimentally attainable conversion. That combination, rather than the isolated use of dark fermentation or of the Gompertz model, defines the novelty space of this study.

The gap addressed by this study lies at the intersection of these three axes and can be expressed in a single proposition: dark fermentation of real mixtures is evaluated using compositional and conversion assumptions that are rarely tested against measured quantities. On the compositional side, mixtures are formulated on a wet basis, and their response is interpreted as though it were additive across the mixed fractions, even though indigenous fermentation causes the outcome to depend on the microbial character contributed by each fraction [32]; the formal framework for testing such additivity, the Scheffé mixture-model framework [33,34], has scarcely been applied to fermentative hydrogen data. On the accounting side, crediting the complete Tier-1 term assumes that diversion destroys the degradable organic carbon (DOC), an assumption that acidogenesis does not satisfy because it removes only a fraction of the carbohydrate pool and returns the remainder in the effluent; two decades of protocol application have documented that the mass-balance method systematically overestimates this effect and that its use outside national inventories requires this limitation to be made explicit [35]. In both cases, the underlying pattern is the same: a qualitative assumption is invoked where a measured quantity that is comparable across systems is required.

To close this gap, a two-component coupled framework is proposed. The first component is an out-of-composition-set mixture-additivity test that calibrates a Scheffé model using the available mixtures and predicts the remaining one, summarizing the deviation through an antagonism index with a bootstrap confidence interval. The second component is a protocol for scaling the avoided-methane credit by an experimentally constrained conversion factor formulated in two tiers: an H_2-based stoichiometric proxy, which is an upper bound because hydrogen carries no carbon, and a carbon-based factor derived from the stoichiometry of the H_2-yielding pathways. The protocol reduces to the conventional credit only when the measured product carries the mineralized carbon, and it can be instantiated for any valorization pathway, not only dark fermentation. Both components are integrated into a four-level hierarchical cascade that preserves mass-flow traceability and explicitly separates experimental assumptions from accounting assumptions.

The working hypothesis is that the fermentative response of a market-waste mixture is not an additive function of its composition and that, consequently, the climate credit derived from this response cannot be scaled according to the diverted mass. The specific objectives testing this hypothesis are: (i) to quantify the generation and composition of the organic waste stream from a district market in Lima and derive the physicochemical properties of mixtures reproducing the recorded generation ratios; (ii) to model the acidogenic gas-production kinetics of four such mixtures in quintuplicate; (iii) to test the additivity of the response and quantify its deviation; and (iv) to close the stoichiometric balance of the hydrogen pathway, propagate its uncertainty, and use this closure to correct the avoided-methane credit.

The contribution is threefold and, in each case, methodological rather than technological. First, the fruit fraction is identified as a necessary condition for acidogenic gas production in market waste over a 72 h timescale, and the response of the fruit-free mixture is shown to fall below every admissible additive expectation, which is the operational definition of antagonism in mixture-design terminology. Second, it is shown that the apparent ranking of mixtures is not preserved across normalization bases, so that the basis of comparison is itself a result. Third, a generalizable accounting correction is provided in which the avoided-methane credit is scaled by the experimentally demonstrated conversion, with its sensitivity decomposed to identify where future analytical effort should be directed. Relative to the closest antecedents, which investigate the ecological consequences of waste mixing [27] or the life-cycle performance of integrated dark-fermentation systems [29,31], the advance lies in the joint use of an out-of-composition additivity test,

a stoichiometric ceiling, and a carbon-consistent credit correction on a mixture whose composition was not designed but inherited from a real waste census. The remainder of the article presents the methodological framework and statistical methods (Section 2), the experimental and accounting results (Section 3), their discussion and limitations (Section 4), and the conclusions (Section 5).

2. Materials and Methods

The study is organized as a four-level hierarchical cascade whose driving variable is the organic waste stream generated by the market (Figure 1). The first level quantifies waste generation and disaggregates it by fraction. The second formulates the mixtures and derives their physicochemical properties. The third resolves batch acidogenic fermentation and its kinetics. The fourth closes the stoichiometric balance and translates the results into carbon accounting. This architecture preserves full traceability of mass flows and explicitly separates experimental assumptions from accounting assumptions.



Figure 1. Hierarchical architecture of the study: six framework stages (F1–F6) with their validation gates (G1–G6), grouped into the four levels described in the text, from the waste-generation census to the carbon-accounting outputs.

The reading of Figure 1 shows why the order of the levels is not arbitrary. The composition of the mixtures at Level 2 is not designed but inherited from the Level 1 census; therefore, the tested points do not form a simplex design, and the mixture model is restricted to first-order terms. In turn, the Level 4 closure depends on a quantity, the volumetric hydrogen fraction, that is not measured at any of the preceding levels, and this dependence is quantified later through the sensitivity analysis. The architecture therefore makes explicit where each assumption enters and which result it propagates to.

2.1. Study Site and Waste-Generation Census

El Pino Market is located in the Carabayllo district, northern Lima, Peru (11.857° S, 77.041° W, WGS84). Ten stalls were monitored for seven consecutive days, from Monday 8 to Sunday 14 September 2025. Waste was collected and weighed daily between 14:00 and 15:00 h using a calibrated platform scale with a resolution of 0.01 kg. The stalls were assigned a priori to three fractions: vegetables, with 2 stalls; fruit, with 2 fruit-selling stalls and 3 juice bars; and cooked food, with 3 prepared-food stalls. The census covers a single week and the selected stalls and does not constitute a seasonally stratified sample, which limits the annualization performed in Section 2.10.

2.2. Sampling and Physicochemical Characterization of Substrates

Composite samples of each fraction were obtained by manually quartering the material accumulated on a single sampling day (5 May 2026), following the national methodological guide for the characterization of municipal solid waste [36]; one 2 kg composite sample was obtained per fraction (laboratory codes MF3, MV2, and MA1 for fruit, vegetables, and cooked food). The samples were homogenized, refrigerated at 4 °C, and delivered within 24 h to an external laboratory (test report IE-0117-0272/26′). Moisture was determined from total solids dried at 103–105 °C, and volatile solids were determined by ignition at 550 °C, both following standardized methods [37]. Carbohydrates were quantified using the phenol–sulfuric acid colorimetric method [38] and reported as milligrams of glucose equivalent per gram of dry matter. A single determination was performed for each fraction; analytical replicates and measurement uncertainties were not reported, and the apostrophe in the test report number denotes parameters outside the laboratory's accreditation scope. The three determinations were performed on the composite sample of each fraction and not on the mixtures; the fraction-level values are listed in Table 1, and all mixture properties reported later are derived from them by mass weighting. The consequences of the absence of analytical replication are treated explicitly in Section 2.12, where assumed analytical uncertainties are propagated to every quantity that depends on these determinations.

Table 1. Physicochemical characterization of the three waste fractions (single determinations on composite samples collected on 5 May 2026; test report IE-0117-0272/26′, moisture by SMEWW 2540 B, volatile solids by SMEWW 2540 E, carbohydrates by the phenol–sulfuric acid method). Dry matter and the wet-basis columns are derived from the reported values.

Fraction	Moisture (%)	Dry Matter (g kg^{-1})	VS (% DM)	Carbohydrates (mg g^{-1} DM)	VS (g kg^{-1} Wet)	Carbohydrates (g kg^{-1} Wet)
Fruit (F, MF3)	81.29	187.1	93.89	522.85	175.7	97.8
Vegetables (V, MV2)	92.04	79.6	81.24	253.39	64.7	20.2
Cooked food (A, MA1)	75.31	246.9	98.04	529.36	242.1	130.7

DM, dry matter; VS, volatile solids. No analytical replicates were run, so no measurement uncertainty is attached to these values; Section 2.12 propagates assumed uncertainties of 0.5 percentage points (moisture), 1.0 percentage point (VS as % DM), and 8% relative (carbohydrates) to the derived quantities.

2.3. Mixture Formulation

Four mixtures were formulated such that the mass ratio of their constituent fractions matched the ratio observed in the generation census: T1 (fruit + vegetables), T2 (vegetables + cooked food), T3 (fruit + cooked food), and T4 (fruit + vegetables + cooked food). The mixtures are therefore points on the composition simplex determined by the waste stream rather than by a simplex-lattice design. The properties of each mixture were calculated by mass weighting, on a wet basis for moisture and on a dry basis for parameters referred to dry matter, using Equation (1)

$$W_{\mathrm{m}} = \sum_i x_i W_i, \qquad \Theta_{\mathrm{m}} = \frac{\sum_i m_i(1 - W_i/100)\Theta_i}{\sum_i m_i(1 - W_i/100)} \tag{1}$$

where the following applies:

W_{m} = Moisture content of the mixture, in %;
Θ_{m} = Value in the mixture of any property referred to dry matter;
x_i = Wet mass fraction of fraction i, dimensionless;
m_i = Mass of fraction i recorded in the generation census, in kg;
W_i = Moisture content of fraction i, in %;
Θ_i = Property of fraction i referred to dry matter, namely volatile solids as % of dry matter or carbohydrates in mg g^{-1} of dry matter.

2.4. Batch Fermentation Experiments

Each mixture was ground and blended to a homogeneous semi-liquid suspension without added water, and its initial pH was adjusted to 5.5 with 1 M HCl or 1 M KOH. Each mixture was fermented in five independent batch reactors, yielding 20 reactors in total, each loaded with 1 kg of wet mixture. The reactors were 1 L Erlenmeyer flasks sealed with rubber stoppers and connected through tubing and a valve to an inverted 500 mL graduated cylinder standing in a water bath; the flasks were wrapped in aluminum foil to exclude light, and their positions were randomized. The reactors operated in batch mode for 72 h at ambient temperature, which ranged between 18 and 25 °C in the laboratory during the campaign but was not logged per reactor, without pH control after the initial adjustment or inoculum addition, relying on the indigenous microbial consortium [32]. Because no water was added, the mixtures as loaded contained between 14.9% and 21.5% total solids, so the reactors operated in the high-solids regime. Cumulative gas volume was recorded every 6 h by displacement of water, refilling the cylinder each time it was full, with a reading resolution of 5 mL, yielding 12 measurements per reactor and 240 observations in total. Gas volumes are reported as measured at laboratory conditions, that is, at ambient temperature and at the atmospheric pressure of Lima (sea level, approximately 101 kPa), and were not corrected to standard temperature and pressure; because the displacement liquid was water rather than an acidified brine, part of the CO_2 dissolved during collection, so the measured volume underestimates the total gas produced while remaining an upper bound on the hydrogen volume, which is practically insoluble. The direction and magnitude of both biases are quantified in Section 2.9. Neither gas composition nor the pH trajectory after the initial adjustment was monitored, and no inoculum blank was run; the consequences of these limitations are addressed in Section 4.8. The measured response is reported throughout the study as cumulative fermentative gas, and quantities expressed in terms of hydrogen are always presented as a bounded interval. Because hydrogen evolution by the acetate and butyrate pathways is always accompanied by CO_2, the absence of gas in a reactor implies the absence of both products; statements about suppression in this study therefore refer to total fermentative gas and not to hydrogen specifically.

2.5. Experimental Conditions of the Photofermentative Stage

A second photofermentative stage was screened using the effluent from the highest-yielding dark-fermentation mixture, produced in a separate 20 L batch run under the same protocol, filtered to remove suspended solids, diluted 1:2, and adjusted to pH 7.5 with 1 M NaOH or 1 M HCl. The stage was run in triplicate, in nine 20 L batch reactors with a working volume of 5 L placed in a 1.20 m × 1.20 m enclosure divided into three compartments and illuminated with LED strips, for 96 h at nominal illuminances of 2500, 3000, and 3500 lx, pH 7.5, and ambient temperature; gas was recorded every 6 h by displacement of a NaOH solution, which absorbs CO_2, so the volumes of this stage are not comparable with those of the dark stage. No inoculum of purple non-sulfur bacteria was added, and irradiance was not measured radiometrically. Illuminance is a photometric quantity weighted by the human photopic response and carries no information on the near-infrared radiation absorbed by bacteriochlorophyll; because the emission spectrum of the source was not recorded, the illuminance values cannot be converted into irradiance, and the stage is not comparable with photofermentation studies reporting W m^{-2}. For this reason, the modified Gompertz equation stage is reported as a negative result in Section 3.6 and is excluded from all yield and emission calculations.

2.6. Data Cleaning and Kinetic Modeling

The cumulative volume is non-decreasing by construction. Two of the 240 readings violated this constraint, both for mixture T3 at 60 h, in replicates 3 and 5, by −5 and −20 mL, respectively. A cumulative-maximum envelope was applied; the effect on the mixture mean was +4 mL kg^{-1}, corresponding to +0.07%. Both the original and corrected values are reported and retained in the Supplementary Dataset S1.

Yields were normalized per gram of added volatile solids rather than per kilogram of wet mixture because the moisture content of the mixtures varied between 78.49% and 85.13%, and wet-basis normalization confounds yield with water content. This is consistent with the requirement imposed by standardized biochemical methane potential protocols for interlaboratory comparability [39,40]. The volatile solids of each mixture were not measured directly but obtained from the fraction-level determinations of Table 1 through Equation (1); the added VS of a reactor is therefore the mass-weighted VS of the 1 kg loaded, and the specific yield is the measured gas volume divided by that quantity.

The cumulative curves were fitted using the modified Gompertz equation [41], given by Equation (2)

$$Y(t) = P \exp\left\{ - \exp\left[\frac{R_m e}{P} (\lambda - t) + 1 \right] \right\} \quad (2)$$

where the following applies:

$Y(t)$ = Cumulative specific gas production at time t, in mL g^{-1} VS;
P = Gas production potential, in mL g^{-1} VS;
R_m = Maximum gas production rate, in mL g^{-1} VS h^{-1};
λ = Lag phase, in h;
t = Fermentation time, in h;
e = Base of the natural logarithm, dimensionless (value: 2.71828).

Equation (2) was fitted to each replicate individually by nonlinear least squares (trust-region reflective algorithm), so that the reported parameters capture the actual dispersion among replicates rather than relying on a single fit to pooled means. The model is used strictly as a descriptive summary of the measured curves: the primary response variable of the study is the measured cumulative yield at 72 h, and the fitted potential P is used only to verify that the assay reached its asymptote. No mechanistic inference is drawn from

the fitted parameters, and the reasons why a structured model such as ADM1 cannot be identified from the present data are discussed in Section 4.5.

2.7. Statistical Analysis

Normality was assessed using the Shapiro–Wilk test, and homogeneity of variances was evaluated using the Brown–Forsythe and Bartlett tests. Because the variance ratio between the extreme groups reached 1137, the classical one-way ANOVA was rejected, and inference was based on the heteroscedastic Welch ANOVA [42], with pairwise Games–Howell comparisons [43]. The Kruskal–Wallis test with the ε^2 effect size is reported as a distribution-free corroboration. Statistical significance was set at $\alpha = 0.05$.

2.8. Mixture Additivity Test

The additivity test asks whether the specific yield of a mixture can be predicted as the blend of the yields of its components. Because the response is expressed per gram of volatile solids, the physically consistent additive expectation is one in which each fraction contributes gas in proportion to the volatile solids it supplies. Compositions were therefore expressed as volatile-solids fractions, $z_i = x_i \mathrm{VS}_i / \sum_j x_j \mathrm{VS}_j$, with VS_i the wet-basis volatile solids of fraction i from Table 1, and a linear Scheffé model [33] was formulated over this composition simplex according to Equation (3)

$$\hat{Y} = \sum_i \beta_i z_i, \qquad \sum_i z_i = 1 \tag{3}$$

where the following applies:

$\hat{Y}$ = Specific gas yield predicted under additivity, in mL g^{-1} VS;
β_i = Linear Scheffé coefficient of component i, in mL g^{-1} VS, interpretable as the specific yield the pure component would exhibit under linear blending;
z_i = Volatile-solids fraction of component i, dimensionless, with i spanning fruit, vegetables, and cooked foods.

Two properties of this formulation are worth stating. First, it is algebraically identical to assuming that each fraction contributes a fixed gas volume per kilogram of its own wet mass, $g_i = \mathrm{VS}_i \beta_i$, so that the predicted volume per kilogram of mixture is $\sum_i x_i g_i$; the antagonism index defined below is consequently independent of the VS determinations themselves. Second, the wet-mass formulation used in the original version of this analysis, in which the VS-normalized response is regressed on wet-mass fractions x_i, is retained as a sensitivity case, because it is the formulation most often encountered in screening studies.

Only four distinct compositions were tested; therefore, the quadratic model is not identifiable [34]. Equation (3) was therefore fitted exactly to the three fruit-containing mixtures, T1, T3, and T4, and used to predict the fruit-free mixture T2, constituting a leave-one-composition-out additivity test. It should be noted that T2 lies on the edge $z_\mathrm{F} = 0$ of the simplex, outside the convex hull of the three calibration points, so the prediction is an extrapolation in the fruit coordinate; the robustness of the conclusion to this extrapolation is examined with two complementary devices described below. The antagonism index is defined by Equation (4)

$$\mathrm{AI} = 100 \cdot \frac{Y_{\mathrm{obs}}(\mathrm{T2})}{\hat{Y}(\mathrm{T2})} \tag{4}$$

where the following applies:

AI = Antagonism index, in %, such that a value of 100% denotes additivity and a value below 100% denotes antagonism;
$Y_{\mathrm{obs}}(\mathrm{T2})$ = Observed specific gas yield of the fruit-free mixture, in mL g^{-1} VS;

$\hat{Y}(\mathrm{T2})$ = Specific gas yield of the fruit-free mixture predicted by Equation (3), in mL g^{-1} VS.

In mixture-design terminology, antagonism denotes a response that falls below the linear-blending expectation, and synergism a response above it [34]; the term is therefore a statement about the shape of the response surface and not about a mechanism. To ensure that the conclusion does not depend on the particular additive null adopted, two additional devices were used. The first is a conservative null in which the vegetable fraction is assumed inert, contributing neither gas nor inhibition; the fruit and cooked-food coefficients are then obtained from T1 and T3 alone, and the fruit-free prediction reduces to the contribution of cooked food. This is the weakest additive expectation compatible with the data, because it credits the fruit-free mixture only with the gas that cooked food produced in the presence of fruit. The second device exploits the maximum higher-order structure that four compositions can support: with the three linear coefficients fixed by T1, T3, and T4, the observed T2 identifies exactly one binary Scheffé interaction term, the vegetable–cooked-food coefficient β_{VA}, through $Y_{\mathrm{obs}}(\mathrm{T2}) = \beta_{\mathrm{V}} z_{\mathrm{V}} + \beta_{\mathrm{A}} z_{\mathrm{A}} + \beta_{\mathrm{VA}} z_{\mathrm{V}} z_{\mathrm{A}}$. This coefficient is the magnitude of the interaction required to reconcile the observation with the linear model; it cannot be validated on independent data, but its sign and its bootstrap interval indicate whether the deviation is of the size and direction of an antagonistic interaction.

Confidence intervals for β_i, $\hat{Y}(\mathrm{T2})$, β_{VA}, and the antagonism index were obtained by nonparametric bootstrap resampling over replicates [44], using 20,000 resamples and a fixed random seed, with replacement within each mixture before refitting the model.

2.9. Stoichiometric and Energy Closure

The upper bound of recoverable hydrogen from the measured carbohydrate pool was taken as the acetate pathway, 4 mol H_2 per mol of hexose [7], according to Equation (5)

$$V_{\mathrm{H_2}}^{\max} = 4 \cdot \frac{C_{\mathrm{carb}}}{M_{\mathrm{hex}}} \cdot V_m \tag{5}$$

where the following applies:

$V_{\mathrm{H_2}}^{\max}$ = Maximum stoichiometric hydrogen volume, in mL kg^{-1} of wet mixture;
C_{carb} = Carbohydrate content of the mixture, in g kg^{-1} of wet mixture;
M_{hex} = Molar mass of hexose, in g mol^{-1} (value: 180.16 g mol^{-1});
V_m = Molar volume of an ideal gas at 273.15 K and 101.325 kPa, in L mol^{-1} (value: 22.414 L mol^{-1}).

Stoichiometric closure is defined as the ratio between the measured hydrogen volume and $V_{\mathrm{H_2}}^{\max}$. Because the gas composition was not measured, two bounding cases are always reported: an upper bound (UB), in which the entire gas phase is hydrogen, and a reference case (RC) at 45% v/v H_2, corresponding to the midpoint of the typical range reported for dark fermentation without pH control on carbohydrate-rich residues [2,3]. Five remarks qualify these bounds. First, the reference case is not a measurement but a literature-based assumption; its role is to place the result within the range of gas compositions commonly reported for mixed-culture fermentation of food waste, and its influence on every downstream quantity is isolated in Sections 2.12 and 3.9. Second, the upper bound is a mathematical envelope rather than a physical state: the gas evolved by the acetate pathway contains at most 66.7% v/v H_2 (4 mol H_2 per 2 mol CO_2), and that of the butyrate pathway is 50%, so hydrogen fractions above two-thirds are possible only if CO_2 is retained in the liquid phase. A stoichiometric bound (SB) at 66.7% v/v is therefore also reported as the highest physically consistent case. Third, the measured volumes refer to laboratory conditions rather than to 273.15 K; for gas saturated with water vapor over the 18–25 °C range recorded in the laboratory, the correction factor to standard conditions lies between 0.92 and 0.89,

so the closure values reported here are overestimated by 6–13%. The correction was not applied because the temperature was not logged per reactor; its direction is conservative with respect to the conclusions of the study, which would be strengthened, not weakened, by it. Fourth, the dissolution of part of the CO_2 in the displacement water means that the collected gas was richer in H_2 than the gas produced; the upper bound remains valid, because hydrogen is practically insoluble, but the stoichiometric bound applies to the gas produced rather than to the gas collected, and the reference case should be read as a composition of the gas produced. Fifth, one bound is independent of composition altogether: the carbon that left the reactor in the collected gas cannot exceed the carbon content of that gas if it were entirely CO_2, $G\,M_C/V_m$, which for the best-performing mixture is 2.93 g C kg^{-1}, or 6.5% of its carbohydrate carbon; this ceiling is used in Section 3.8 to bound the credit without any assumption about the hydrogen fraction.

Energy recovery compares the lower heating value of hydrogen, 120 MJ kg^{-1} at a density of 0.08988 kg m^{-3}, with a substrate chemical energy content of 17 MJ kg^{-1} VS. The latter value is consistent with the composition of the volatile solids: the lower heating value of hexose is 14.1 MJ kg^{-1} (combustion enthalpy of 2803 kJ mol^{-1} less the latent heat of the water formed), whereas proteins and lipids lie near 22 and 37 MJ kg^{-1}, so a carbohydrate-dominated VS pool falls in the 15–19 MJ kg^{-1} range; adopting 20 MJ kg^{-1} VS instead would lower every recovery figure by 15% without altering any ranking. The methanogenic reference was calculated for biochemical methane potentials of 350 and 400 L CH_4 kg^{-1} VS, using a methane density of 0.7168 kg m^{-3} and a lower heating value of 50 MJ kg^{-1}.

To trace the fate of the carbon and energy that do not leave the process as hydrogen, a stoichiometric partition was constructed for the best-performing mixture. For a given hydrogen fraction, the moles of H_2 fix the moles of hexose converted through the yield of the pathway, 4 mol H_2 per mol hexose for acetate and 2 for butyrate; each converted hexose releases 2 mol of carbon as CO_2 and retains 4 mol of carbon in the acid. Carbon that is neither in the gas nor in the acids is assigned to unconverted carbohydrate, and the carbon of the non-carbohydrate volatile solids, which were not speciated, is estimated at 0.5 g C per gram of VS. The energy partition uses the lower heating values of hydrogen (120.0 MJ kg^{-1}), acetic acid (13.1 MJ kg^{-1}), butyric acid (22.8 MJ kg^{-1}), and hexose (14.1 MJ kg^{-1}), and assigns the balance of the 17 MJ kg^{-1} VS to the non-carbohydrate fraction. The partition is evaluated for the reference case and for the stoichiometric bound, and for the acetate and butyrate pathways as limiting cases; any CO_2 in the gas phase in excess of what the H_2-yielding pathway implies is attributed to routes that release CO_2 without hydrogen, such as the ethanol-type and lactate-to-propionate fermentations.

2.10. Avoided-Methane Accounting

Methane from the baseline disposal pathway was estimated using the IPCC default mass-balance equation [19], given by Equation (6)

$$CH_4 = MSW_T \cdot MSW_F \cdot MCF \cdot DOC \cdot DOC_F \cdot F \cdot \frac{16}{12} \cdot (1 - R)(1 - OX) \quad (6)$$

where the following applies:

CH_4 = Baseline methane generation, in t $year^{-1}$;
MSW_T = Mass of waste diverted from final disposal, in t $year^{-1}$;
MSW_F = Fraction of waste disposed of under the baseline scenario, dimensionless (adopted value: 1.0);
MCF = Methane correction factor, dimensionless (adopted value: 0.6, the IPCC default for uncategorized solid waste disposal sites, adopted because the depth and management of

the dumpsites receiving Lima's uncollected market waste are not documented, a limitation also reported for the national inventory of critical dumpsites [6]);
DOC = Degradable organic carbon, in t C t^{-1} of waste on a wet basis (adopted value: 0.15, the IPCC wet-basis default for food waste, which implies a moisture content of about 60%; [20]);
DOC_F = Fraction of degradable organic carbon that decomposes, dimensionless (adopted value: 0.6);
F = Volumetric fraction of methane in landfill gas, dimensionless (adopted value: 0.5);
16/12 = Stoichiometric conversion factor from carbon to methane, dimensionless;
R = Recovered methane, dimensionless (adopted value: 0);
OX = Oxidation factor, dimensionless (adopted value: 0).

The default parameters were retained deliberately, because the object of the correction developed below is the credit that practitioners actually compute with them. Two of the defaults are, however, generous for this substrate: an unmanaged shallow site would take MCF = 0.4, and the IPCC dry-basis default for food waste, 0.38 t C t^{-1} DM, applied to the measured dry matter of the mixture gives DOC = 0.082 instead of 0.15. The effect of both alternatives on the baseline is quantified in Section 3.8.

Credits are reported using the AR5 metric, for which the 100-year global warming potential is 28, and the AR6 metric for non-fossil methane, for which it is 27 [45]. The conversion-scaled credit introduced in this work is defined by Equations (7) and (8)

$$\mathrm{Credit}_{\mathrm{scaled}} = \eta \cdot \mathrm{CH_4} \cdot \mathrm{GWP}_{100} \tag{7}$$

$$\eta_{\mathrm{H_2}} = \frac{V_{\mathrm{H_2}}^{\mathrm{meas}}}{V_{\mathrm{H_2}}^{\mathrm{max}}} \tag{8}$$

where the following applies:

$\mathrm{Credit}_{\mathrm{scaled}}$ = Avoided emissions attributable to the diversion scheme, in t CO_2eq $year^{-1}$.
η = Effective conversion factor, dimensionless; instantiated either as the H_2-based proxy $\eta_{\mathrm{H_2}}$ or as the carbon-based factor η_{C} defined in Equation (9).
$\eta_{\mathrm{H_2}}$ = Proxy factor for effective conversion inferred from the H_2-based stoichiometric closure; dimensionless; it does not represent a direct measurement of carbon removal.
$V_{\mathrm{H_2}}^{\mathrm{meas}}$ = Measured hydrogen volume under the assumed gas composition, in mL kg^{-1}.
GWP_{100} = 100-year global warming potential of methane, in kg CO_2eq kg^{-1} CH_4.

Hydrogen carries no carbon, so $\eta_{\mathrm{H_2}}$ measures the fraction of the carbohydrate pool that was converted along the H_2-yielding pathway rather than the fraction of carbon removed from the methanogenic pool. In both the acetate and the butyrate pathways, one third of the carbon of each converted hexose is mineralized to CO_2 and two thirds remain in the effluent as acid, which is fully methanogenic under anaerobic disposal. The carbon-based conversion factor consistent with a given H_2 closure is therefore given by Equation (9)

$$\eta_{\mathrm{C}} = \frac{4}{3\,Y_{\mathrm{H_2}}}\,\eta_{\mathrm{H_2}} \tag{9}$$

where the following applies:

η_{C} = Fraction of the carbohydrate carbon mineralized to CO_2, dimensionless.
$Y_{\mathrm{H_2}}$ = Hydrogen yield of the pathway, in mol H_2 mol^{-1} hexose; four for the acetate pathway and two for the butyrate pathway, giving $\eta_{\mathrm{C}} = \eta_{\mathrm{H_2}}/3$ and $2\eta_{\mathrm{H_2}}/3$, respectively.

Equation (7) establishes the physical requirement that unconverted carbon cannot be credited as avoided. Fossil-fuel substitution was evaluated using the IPCC default

emission factors of 56.1 for natural gas, 69.3 for gasoline, 74.1 for diesel and gas oil, and 94.6 kg CO_2 GJ^{-1} for bituminous coal [20].

2.11. Measured-Conversion Credit Scaling Protocol

Equation (7) is not an ad hoc adjustment for this dataset, but rather a particular instance of a general protocol that is explicitly formulated here so that it can be applied to other pathways and systems. The protocol consists of four steps.

Step 1. Establish the baseline. Estimate the methane that the diverted mass would have generated under the final-disposal scenario using Equation (6), explicitly stating the method employed and its parameters.

Step 2. Determine the conversion ceiling. Calculate the maximum amount of gaseous product that the degradable fraction of the substrate could yield under the stoichiometry of the pathway considered. For dark fermentation, this ceiling is given by Equation (5).

Step 3. Measure the effective conversion. Quantify the product actually obtained and express it as a fraction of the ceiling established in the previous step, according to Equation (8). When any quantity required for this ratio has not been measured, as is the case here for gas composition, a bounded interval rather than a point estimate must be reported. When the measured product does not carry carbon, as with hydrogen, the ratio must be translated into a carbon-based factor through the pathway stoichiometry, as in Equation (9).

Step 4. Scale the credit. Multiply the baseline by the effective conversion using Equation (7) and propagate the uncertainty of all parameters involved.

Three properties of the protocol are worth highlighting. The first is its consistency in the limiting case: when the measured product carries the mineralized carbon, as methane does in anaerobic digestion or CO_2 in composting, complete conversion gives a scaling factor of unity, and the result coincides exactly with the conventional credit, so the protocol does not penalize pathways that actually mineralize the carbon. For dark fermentation, this limit is not attainable even in principle: complete conversion along the acetate pathway mineralizes only one third of the carbohydrate carbon, so the H_2-based proxy overstates the carbon mineralized along the H_2-yielding pathways by a factor of 1.5 to 3. Routes that release CO_2 without hydrogen add to the mineralized carbon, but the total is bounded, for any gas composition, by the carbon content of the collected gas. The second is its transferability: effective conversion is instantiated differently depending on the pathway, as summarized in Table 2, but the calculation structure remains unchanged. The third is its conservative character with respect to the correction: the protocol scales the credit according to the conversion of carbon to gaseous product and does not deduct process energy consumption or emissions associated with the remaining effluent; consequently, the corrected credit remains an upper bound on the net benefit.

Table 2. Instantiation of effective conversion in the scaling protocol according to the valorization pathway.

Valorization Pathway	Measured Product	Stoichiometric Ceiling	Effective Conversion
Dark fermentation	H_2 (carbon-free)	4 mol H_2 mol^{-1} hexose	η_{H_2} = Measured/ceiling (upper bound); $\eta_C = \eta_{H_2}/3$ to $2\eta_{H_2}/3$
Anaerobic digestion	CH_4	Biochemical methane potential	yield/BMP
Composting	Mineralized CO_2	Degradable organic carbon	mineralized C/DOC
Lactic fermentation	Lactate	2 mol lactate mol^{-1} hexose	no conversion to gas

DOC, degradable organic carbon; BMP, biochemical methane potential. The last row illustrates the limiting case: a pathway that does not mineralize carbon to the gas phase does not generate an avoided-methane credit by itself, regardless of the mass diverted.

It should also be noted what the protocol does not do. It does not replace a life-cycle assessment nor does it attempt to close the process net-energy balance; it does not resolve emission timing, for which a first-order decay model would be required; and it does not assign any credit to carbon that remains in the effluent, whose fate must be reported separately. Its scope is deliberately limited: to prevent carbon from being credited as avoided when no measurement demonstrates that it has been converted.

2.12. Monte Carlo Uncertainty Propagation

To quantify how parameter uncertainty propagates to the corrected credit, a Monte Carlo simulation with $N = 10{,}000$ independent realizations was performed. The sampling employed differentiated prior distributions according to the nature of the available information: normal distributions where a central estimate with known dispersion was available, and uniform distributions where only an admissible range was known without a preferred modal value. Carbohydrates were sampled as $\mathcal{N}(113.22,\ 9.06)$ g kg^{-1}, corresponding to a coefficient of variation of 8%, consistent with a single determination without replication; measured gas was sampled as $\mathcal{N}(5469,\ 104)$ mL kg^{-1}, using the experimental standard deviation among replicates; and the following variables were sampled as uniform distributions: the volumetric hydrogen fraction $\mathcal{U}(0.35,\ 0.55)$, degradable organic carbon $\mathcal{U}(0.13,\ 0.17)$, the methane correction factor $\mathcal{U}(0.50,\ 0.70)$, the degradable fraction $\mathcal{U}(0.50,\ 0.70)$, and the global warming potential $\mathcal{U}(26,\ 29)$. The efficiency in Equation (8) was recalculated endogenously in each realization, so that the stoichiometric constraint was consistently enforced throughout the entire propagation. Because the hydrogen fraction is the only parameter that was neither measured nor drawn from an inventory default, the propagation was repeated with a narrow prior, $\mathcal{U}(0.40,\ 0.50)$, and a wide prior, $\mathcal{U}(0.25,\ 0.667)$, whose upper limit is the stoichiometric bound of the acetate pathway; the three runs quantify how the interval of the overestimation factor responds to the assumed range of gas composition. The DOC prior spans only the neighborhood of the wet-basis default; the substrate-specific alternative of Section 2.10 is treated as a separate scenario rather than as part of the prior.

A second propagation addresses the absence of analytical replication in the substrate characterization. Assumed analytical uncertainties were assigned to each fraction-level determination of Table 1: a standard deviation of 0.5 percentage points for moisture, 1.0 percentage point for volatile solids as a fraction of dry matter, and a relative standard deviation of 8% for carbohydrates, sampled independently for the three fractions in 20,000 realizations. Every quantity derived from these determinations, namely the mixture properties, the specific yields, the VS fractions z_i, the mixture-model prediction, the stoichiometric ceiling, and the closure, was recomputed in each realization.

The point estimator and the 95% uncertainty interval for any output variable were obtained using Equations (10) and (11). The interval is the empirical range between the 2.5th and 97.5th percentiles of the propagated distribution; it is an uncertainty interval rather than a frequentist confidence interval, because it quantifies the dispersion induced by the assumed prior distributions rather than the sampling variability of an estimator

$$\hat{Z} = \frac{1}{N}\sum_{i=1}^{N} Z_i \tag{10}$$

$$\mathrm{UI}_{95\%} = \left[Z_{(0.025\cdot N)},\ Z_{(0.975\cdot N)}\right] \tag{11}$$

where the following applies:

$\hat{Z}$ = Point estimator, sample mean of the output variable;
Z_i = Value of the output variable in realization i;

N = Total number of Monte Carlo realizations, dimensionless (value: 10,000);
$UI_{95\%}$ = Empirical 95% uncertainty interval, defined by the 2.5th and 97.5th percentiles.

2.13. Global Sobol Sensitivity Analysis

To identify which parameters dominate the variance of the corrected credit, a Sobol variance-based decomposition was performed [46,47]. Samples were generated with the Saltelli scheme and the indices estimated with the Jansen estimators as implemented in the SALib library [48]. The total number of model evaluations was $N_{\text{total}} = N_{\text{base}} \cdot (D + 2)$, with $N_{\text{base}} = 16{,}384$ and $D = 7$ parameters, resulting in 147,456 model evaluations; bootstrap confidence intervals of the indices were obtained from 100 resamples. The first-order sensitivity index for each parameter was calculated using Equation (12)

$$S_i = \frac{\text{Var}_{X_i}\left[\mathbb{E}_{X_{\sim i}}(Z \mid X_i)\right]}{\text{Var}(Z)} \tag{12}$$

where the following applies:

S_i = First-order sensitivity index of parameter X_i, dimensionless;
Z = Output variable of the model, here the conversion-scaled credit, in t CO_2eq year^{-1};
$X_{\sim i}$ = Set of all parameters other than X_i.

The total-order index, which captures both the direct effect and the interactions of the parameter with the other parameters, was calculated using Equation (13)

$$S_{Ti} = 1 - \frac{\text{Var}_{X_{\sim i}}\left[\mathbb{E}_{X_i}(Z \mid X_{\sim i})\right]}{\text{Var}(Z)} \tag{13}$$

where the following applies:

S_{Ti} = Total-order sensitivity index of parameter X_i, dimensionless.

Parameters with $S_{Ti} > 0.10$ were considered dominant contributors to model variability.

2.14. Computational Implementation

The kinetic fits, statistical tests, bootstrap resampling, and accounting balances were implemented in Python 3 using open-source scientific libraries: NumPy [49] for vectorized numerical operations, SciPy [50] for the trust-region nonlinear least-squares fitting of Equation (2) and for hypothesis testing, SALib [48] for the Sobol decomposition, and Matplotlib [51] for scientific visualization. All stochastic routines were executed with a fixed random seed, so that the bootstrap intervals reported in Section 3.5 result from a single deterministic run. The analysis script, figure-generation script, and cleaned dataset are provided as Supplementary Materials.

2.15. Classification of Reported Quantities

Because the study combines measured, fitted, assumed, and derived quantities, and because the accounting conclusions depend on some of the latter, Table 3 classifies every quantity reported in Section 3 by its epistemic status. Only the first group is experimental evidence in the strict sense; the second is a descriptive summary validated against the first; the third consists of declared assumptions whose influence is propagated in Sections 2.12 and 2.13; and the fourth follows from the previous three by arithmetic.

Table 3. Epistemic status of the quantities reported in this study.

Status	Quantities	Validation or Treatment
Measured	Daily waste generation by stall; fraction-level moisture, VS and carbohydrates (single determinations); initial pH of each reactor (adjusted to 5.5); cumulative gas volume at 6 h intervals in 20 reactors; photofermentation gas volume	Direct observation; gas replicated in quintuplicate; substrate characterization not replicated (uncertainty propagated, Section 2.12)
Fitted	Modified Gompertz parameters P, R_m, λ; linear Scheffé coefficients β_i; interaction coefficient β_{VA}	Gompertz: per-replicate least squares, R^2 and RMSE against the measured curves, P checked against the measured 72 h yield; Scheffé: exact fit to three compositions, out-of-composition prediction of the fourth, bootstrap intervals
Assumed	Volumetric H_2 fraction (RC, SB, UB); IPCC default parameters (MCF, DOC, DOC_F, F); substrate energy content; carbon content of non-carbohydrate VS; analytical uncertainties of the single determinations	Declared with their source; propagated by Monte Carlo with three priors for the H_2 fraction; ranked by Sobol indices; alternative defaults evaluated as scenarios
Derived	Mixture properties; specific yields; $V_{H_2}^{max}$; closure; η_{H_2} and η_C; energy recovery; baseline methane; scaled credits; carbon and energy partition	Arithmetic from the previous groups; reproducible from the Supplementary Dataset S1

3. Results

3.1. Waste Generation and Composition

The 10 monitored stalls generated 754.6 kg over the census week, as shown in Figure 2a. Daily generation ranged from a midweek minimum of 91.6 kg on Wednesday to a weekend maximum of 126.1 kg on Saturday, with 120.3 kg on Sunday. Fruit waste dominated with 309.7 kg, corresponding to 41.04%, followed by cooked food waste with 272.7 kg or 36.14%, and vegetables with 172.2 kg or 22.82%, as summarized in Figure 2b. Aggregation by fraction reproduced the stall-level data with a deviation below 0.03 kg on every day of the census.

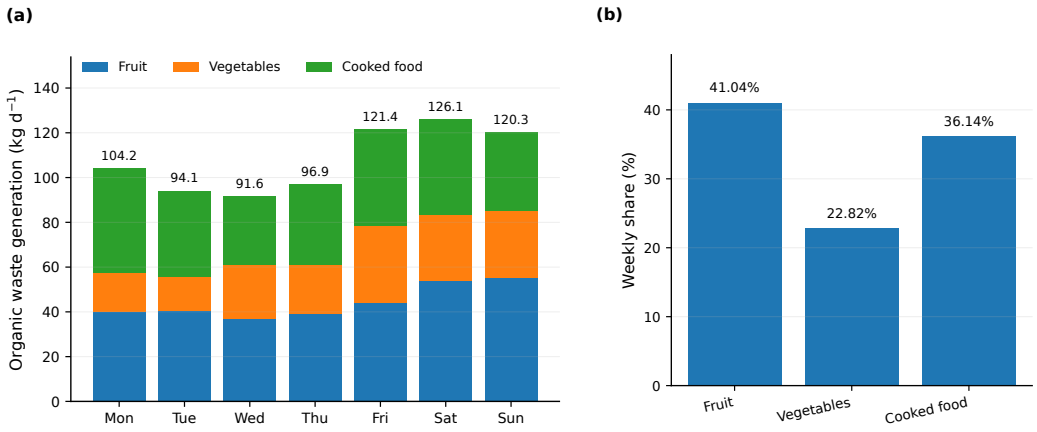

Figure 2. Organic waste generation at the El Pino market, Carabayllo, Lima: (**a**) daily generation disaggregated by fraction, with the daily total indicated above each bar; (**b**) contribution of each fraction to the weekly total, in %. Ten stalls were monitored for seven consecutive days.

Two features of Figure 2 condition the remainder of the study. The first is the dominant position of fruit, which not only accounts for the largest share of waste generation but also determines its presence in three of the four tested mixtures and, as shown below, dominates the fermentation response. The second is the spread between the Wednesday minimum and the Saturday maximum, 34.5 kg, corresponding to 38% above the minimum value, which indicates that annualizing a single week to 52 weeks is a simplification rather than a

measurement. The composition shown in Figure 2b, by contrast, is transferred directly to the mass fractions of Table 4.

Table 4. Composition and physicochemical properties of the four mixtures. Wet-basis mass fractions are derived from the generation census; properties are mass-weighted from the single laboratory determinations of Table 1 using Equation (1).

Mixture	x_F	x_V	x_A	Moisture (%)	VS (g kg^{-1})	Carbohydrates (mg g^{-1} DM)
T1	0.643	0.357	—	85.13	136.0	471.3
T2	—	0.387	0.613	81.79	173.4	482.7
T3	0.532	—	0.468	78.49	206.8	526.3
T4	0.410	0.228	0.361	81.58	174.3	499.4

Mixtures: T1, fruit + vegetables; T2, vegetables + cooked food; T3, fruit + cooked food; T4, fruit + vegetables + cooked food. F, fruit; V, vegetables; A, cooked food; DM, dry matter; VS, volatile solids. Dry matter is obtained from moisture as $(100 - W_m) \times 10$ g kg^{-1}, yielding 148.7, 182.1, 215.1, and 184.2 g kg^{-1} for T1 to T4. Volatile solids as a fraction of dry matter are 91.47%, 95.20%, 96.12%, and 94.65%, respectively. The corresponding volatile-solids fractions (z_F, z_V, z_A) used in Section 3.5 are (0.830, 0.170, —), (—, 0.144, 0.856), (0.452, —, 0.548), and (0.414, 0.085, 0.502).

3.2. Mixture Properties

The properties of the mixtures derived from Equation (1) are presented in Table 4. The fruit-free mixture T2 is not carbohydrate-poor: at 482.7 mg g^{-1} dry matter, its carbohydrate concentration is marginally higher than that of T1, which is 471.3, and only 8.3% lower than that of T3, which is 526.3. On a wet basis, T2 provides more volatile solids, 173.4 g kg^{-1}, than T1, which provides 136.0 g kg^{-1}. Therefore, any explanation of the fermentation results based solely on substrate concentration can be ruled out from the outset. Table 4 also admits a second interpretation: moisture varies by 6.6 percentage points between T3 and T1, which is sufficient for a yield expressed on a wet basis to incorporate a water-content term unrelated to fermentation. This is why the entire following section is expressed per gram of volatile solids.

The fraction-level values of Table 1 add a third reading. The vegetable fraction supplies only 64.7 g VS kg^{-1} and 253.5 mg of carbohydrates per gram of dry matter, less than half the values of the other two fractions; expressed as volatile-solids fractions, vegetables account for 17.0% of the VS of T1, 14.4% of T2, and 8.5% of T4, whereas cooked food accounts for 85.6% of the VS of T2. Whatever suppresses the fruit-free mixture therefore acts on a substrate that is, by mass of volatile solids, almost entirely cooked food, the same fraction that ferments readily in T3.

3.3. Gas Production Kinetics

The cumulative curves and their Gompertz fits are presented in Figure 3, and the fitted parameters are given in Table 5. The model closely described all four mixtures, with mean R^2 values ranging from 0.982 to 0.994 and per-replicate root-mean-square errors between 0.018 and 0.991 mL g^{-1} VS.

The specific yields at 72 h ranked T3 above T1 and T4, which in turn were substantially higher than T2, with values of 26.45 ± 0.50, 18.89 ± 0.97, 18.41 ± 0.07, and 0.63 ± 0.03 mL g^{-1} VS, respectively. The Welch ANOVA rejected equality of means, with $F_{3,7.32} = 8.65 \times 10^4$ and $p = 5.3 \times 10^{-17}$, corroborated by the Kruskal–Wallis test with $H = 16.75$, $p = 7.9 \times 10^{-4}$, and $\varepsilon^2 = 0.860$. Games–Howell comparisons separated all pairs at $p < 0.001$, with the sole exception of T1 versus T4, for which $p = 0.713$. The suppression of T2 relative to T3 is quantified as the ratio of the measured 72 h specific yields, $26.45/0.63 = 41.7$, with a 95% bootstrap interval of 40.2 to 43.4 obtained by resampling the five replicates of each mixture; the ratio of the fitted Gompertz potentials,

$26.68/0.66 = 40.4$, is consistent with it. The ratio refers to total fermentative gas, not to hydrogen.

This exception is relevant. On a wet-mass basis, T4 appears clearly superior to T1, with 3210 versus 2569 mL kg^{-1}, a 25% difference, and the ternary mixture would therefore be selected as the best three-component formulation. When normalized per gram of added volatile solids, however, the two mixtures are statistically indistinguishable, and the apparent superiority is an artifact of the 38 g kg^{-1} difference in volatile-solids loading. Only T3 is genuinely superior.

Figure 4 compares the specific yield with the fitted potential and maximum production rate for the four mixtures. The maximum production rate followed the same ranking as the potential P, with values of 0.915 for T3, 0.709 for T1, 0.575 for T4, and 0.017 mL g^{-1} VS h^{-1} for T2, with a Welch statistic of $F_{3,6.69} = 738.8$ and $p = 8.4 \times 10^{-9}$. The fitted lag phases were negative for all mixtures, ranging from -2.44 to -0.59 h, which is not physically interpretable and indicates that gas evolution had already begun before the first measurement at 6 h. The sampling grid is therefore too coarse to resolve λ, and these values should be interpreted as evidence of an immediate onset rather than as estimates.

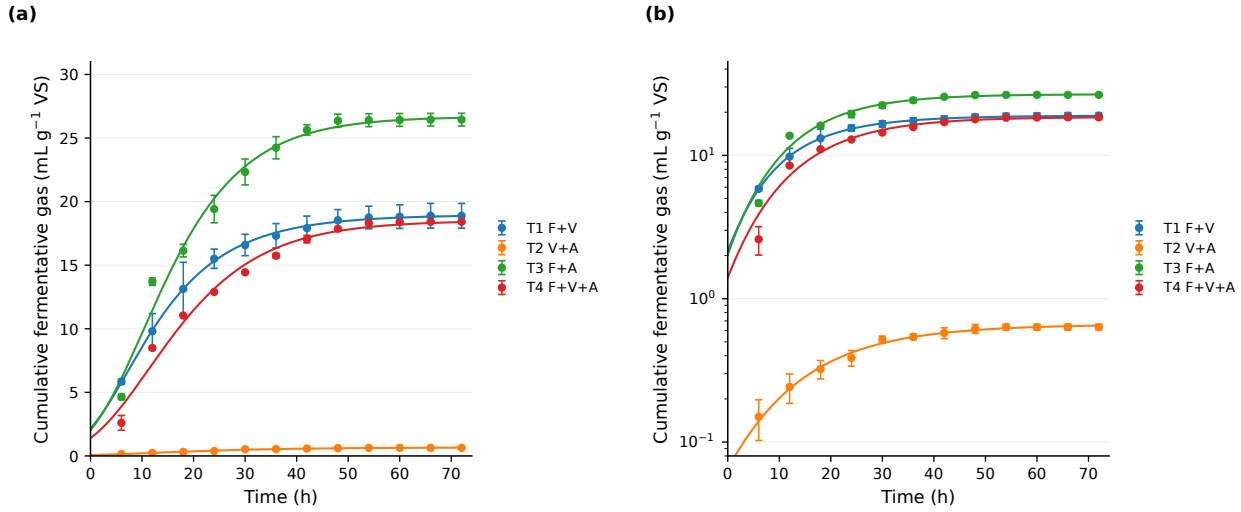

Figure 3. Cumulative fermentative gas production normalized per gram of added volatile solids: (**a**) linear scale; (**b**) logarithmic scale. Symbols represent means of five independent reactors, error bars denote standard deviations, and lines are modified Gompertz fits obtained using Equation (2), for which R^2 ranges from 0.982 to 0.994. The fruit-free mixture T2 is suppressed by a factor of 41.7 (95% bootstrap interval 40.2–43.4) relative to T3, computed from the measured 72 h yields.

Table 5. Modified Gompertz parameters, reported as mean ± standard deviation of five independent fits per mixture, and cumulative yields at 72 h. R^2 is the mean of the five per-replicate fits.

Mixture	P (mL g^{-1} VS)	R_m (mL g^{-1} VS h^{-1})	λ (h)	R^2	Y_{72} (mL g^{-1} VS)	Y_{72} (mL kg^{-1})
T1 (F + V)	18.96 ± 1.11	0.709 ± 0.164	-2.44 ± 1.62	0.994	18.89 ± 0.97 [a]	2569 ± 132
T2 (V + A)	0.66 ± 0.04	0.017 ± 0.002	-2.09 ± 3.31	0.982	0.63 ± 0.03 [c]	110 ± 5
T3 (F + A)	26.68 ± 0.44	0.915 ± 0.071	-0.59 ± 0.60	0.982	26.45 ± 0.50 [b]	5469 ± 104
T4 (F + V + A)	18.50 ± 0.12	0.575 ± 0.030	-0.61 ± 0.94	0.983	18.41 ± 0.07 [a]	3210 ± 12

Superscript letters denote Games–Howell groups for specific yield at $\alpha = 0.05$; mixtures sharing a letter do not differ significantly.

Table 5 provides an interpretation that the means alone do not reveal. The potential P and the observed yield at 72 h agree across all four mixtures within a difference of less than 0.4%, indicating that the assay effectively reached the asymptote and that the 72 h endpoint did not truncate production. Furthermore, T1 and T4 share similar potentials but differ in maximum production rate, 0.709 versus 0.575 mL g^{-1} VS h^{-1}: the ternary mixture reaches the same endpoint more slowly, which is consistent with the vegetable fraction diluting the kinetics without altering the ceiling. In T2, by contrast, the kinetics are not merely slow: the potential itself collapses to 0.66 mL g^{-1} VS, indicating that the problem is not one of rate but of metabolic pathway.

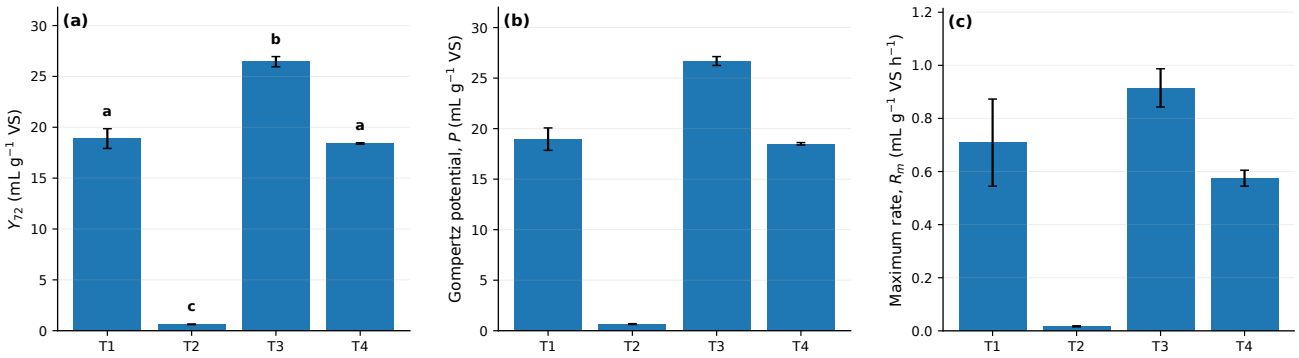

Figure 4. (**a**) Cumulative specific gas yield at 72 h; (**b**) Gompertz production potential P; (**c**) maximum production rate R_m. Bars represent means of five independent reactors, and error bars denote standard deviations. Letters in (**a**) denote Games–Howell groups at $\alpha = 0.05$.

The comparison of the three panels in Figure 4 separates two questions that are often conflated. Figure 4a,b are practically superimposable, confirming that the observed yield and the fitted potential measure the same quantity in this experiment. Figure 4c is the one that adds information: the ordering of the maximum production rate coincides with that of the potential except for the T1–T4 pair, whose heights are equalized in Figure 4a,b but separated in Figure 4c. The error bars are also informative in their own right: the dispersion of R_m in T1 is the largest in the dataset, indicating that the initial kinetics of the fruit–vegetable mixture are the least reproducible, whereas those of T4 are anomalously small, an issue revisited in Section 4.8.

3.4. Verification of Assumptions and Statistical Tests

Before any statistical test, the distributional assumptions and homogeneity of variances were assessed; the results are summarized in Table 6. The Shapiro–Wilk test rejects normality only for T1, whereas the remaining three mixtures are compatible with normality. The decisive diagnosis, however, concerns the variances: the Brown–Forsythe test does not reject homogeneity, whereas Bartlett's test does so strongly, and the ratio between the largest and smallest variances reaches 1137.

This discrepancy between the two tests is interpretable and not contradictory. Brown–Forsythe is deliberately robust and loses power with five replicates per group, whereas Bartlett's test is sensitive precisely to the situation observed here, in which the variances differ by three orders of magnitude because T2 and T4 are nearly deterministic compared with T1. With a variance ratio of 1137, the classical one-way ANOVA is not admissible regardless of the outcome of either test, and therefore all subsequent inference is based on Welch's procedure.

Table 6. Verification of assumptions for the specific yield at 72 h and global statistical tests.

Mixture	Mean (mL g^{-1} VS)	SD (mL g^{-1} VS)	CV (%)	Shapiro–Wilk	
				W	*p*
T1	18.89	0.972	5.15	0.686	0.0068
T2	0.63	0.029	4.55	0.821	0.1185
T3	26.45	0.502	1.90	0.920	0.5329
T4	18.41	0.067	0.37	0.813	0.1033

Homogeneity of variances: Brown–Forsythe $W = 1.478$, $p = 0.2583$; Bartlett $\chi^2 = 33.02$, $p = 3.18 \times 10^{-7}$; maximum-to-minimum variance ratio = 1137. Global tests: Welch's ANOVA $F_{3,7.32} = 8.65 \times 10^4$, $p = 5.30 \times 10^{-17}$, $\omega^2 = 0.9967$; Kruskal–Wallis $H = 16.75$, $p = 7.9 \times 10^{-4}$, $\varepsilon^2 = 0.860$. SD, standard deviation; CV, coefficient of variation.

Both global tests agree in rejecting equality of means, and the effect sizes are extraordinarily large: an ω^2 of 0.9967 indicates that mixture identity explains virtually all of the variance in yield. Nevertheless, this magnitude should not be overinterpreted: with four treatments whose means range from 0.63 to 26.45 mL g^{-1} VS and with minimal within-group dispersion, an ω^2 close to unity was an expected outcome and does not constitute additional evidence.

The Games–Howell pairwise comparisons are presented in Table 7. Five of the six pairs differ at $p < 0.001$; the only exception is T1 versus T4, whose difference of +0.48 mL g^{-1} VS does not reach statistical significance. This conclusion does not depend on the anomalously small dispersion of T4 discussed in Section 4.8: if the standard deviation of T4 is inflated to the coefficient of variation of T2 (4.55%) or of T1 (5.15%), the Games–Howell probability for the T1–T4 pair rises to 0.84 and 0.86, respectively, because the Welch statistic is dominated by the dispersion of T1. The remaining five pairs stay separated at $p < 0.001$ under the same inflation.

Table 7. Games–Howell pairwise comparisons for the specific yield at 72 h, with Cohen's effect size.

Pair	Difference (mL g^{-1} VS)	df	*p*	Cohen's *d*
T1 vs T2	+18.25	4.01	<0.001	+26.54
T1 vs T3	−7.56	5.99	<0.001	−9.77
T1 vs T4	+0.48	4.04	0.7126	+0.69
T2 vs T3	−25.82	4.03	<0.001	−72.55
T2 vs T4	−17.78	5.42	<0.001	−343.53
T3 vs T4	+8.04	4.14	<0.001	+22.43

df, Welch–Satterthwaite degrees of freedom. Effect sizes for pairs involving T4 should be interpreted with caution: the anomalously small standard deviation of this mixture, discussed in Section 4.8, reduces the denominator of *d* and produces values lacking physical interpretability, such as that for T2 versus T4.

3.5. Non-Additivity of the Mixture Response

The linear Scheffé model formulated on volatile-solids fractions and calibrated on T1, T3, and T4 using Equation (3) yielded a fruit coefficient of 36.76, with a 95% bootstrap confidence interval of 35.41 to 37.95; a cooked-food coefficient of 17.95, with an interval of 17.41 to 18.83; and a vegetable coefficient of −68.38, with an interval of −72.63 to −64.09 mL g^{-1} VS, as shown in Figure 5b. The vegetable coefficient was negative in 100% of the 20,000 bootstrap resamples.

Applied to the fruit-free composition, the model predicts 5.48 mL g^{-1} VS, with a 95% confidence interval of 4.62 to 6.45, whereas the observed value was 0.63 mL g^{-1} VS. The antagonism index defined by Equation (4) is therefore 11.6%, with a 95% confidence interval of 9.8% to 13.7%, corresponding to an 88.4% suppression of total fermentative gas relative to the additive expectation, and the bootstrap probability that the index is below 100% is unity. Removing the fruit fraction does not reduce the response in proportion to the mass or carbohydrates removed; it suppresses fermentation.

Table 8 shows that this conclusion is not a property of the particular additive null adopted. The wet-mass formulation of the original analysis predicts 7.39 mL g^{-1} VS and gives an index of 8.6%; the conservative null that treats vegetables as inert, and therefore credits the fruit-free mixture only with the gas that cooked food produced in the presence of fruit, predicts 25.2 mL g^{-1} VS on a VS basis and 14.2 on a wet basis, giving indices of 2.5% and 4.5%. Across all admissible specifications, the index lies between 2.5% and 13.7%, so the weakest statement supported by the data is that the fruit-free mixture produced less than one seventh of any additive expectation. The binary interaction coefficient that reconciles the observation with the linear model, $\beta_{VA} = -39.2$ mL g^{-1} VS with a bootstrap interval of −47.0 to −32.3, is negative in every resample and exceeds the cooked-food linear coefficient in magnitude; in the language of mixture design, the vegetable–cooked-food blend behaves antagonistically, and the interaction required to explain it is of the same order as the main effects.

Table 8. Mixture-model results under alternative specifications of the additive null. Coefficients in mL g^{-1} VS; brackets are 95% bootstrap intervals from 20,000 resamples.

Specification	β_F	β_V	β_A	$\hat{Y}$ (T2)	AI (%)	β_{VA}
VS-fraction basis (primary)	36.76 [35.41, 37.95]	−68.38 [−72.63, −64.09]	17.95 [17.41, 18.83]	5.48 [4.62, 6.45]	11.6 [9.8, 13.7]	−39.2 [−47.0, −32.3]
Wet-mass basis (sensitivity)	34.25 [32.73, 35.49]	−8.74 [−10.08, −7.38]	17.58 [16.63, 19.13]	7.39 [6.52, 8.47]	8.6 [7.5, 9.8]	−28.5 [−33.0, −24.8]
Vegetables inert, VS basis	22.76	0	29.49	25.2	2.5	—
Vegetables inert, wet basis	29.39	0	23.10	14.2	4.5	—

AI, antagonism index (Equation (4)); β_{VA}, vegetable–cooked-food binary interaction coefficient identified from the observed T2 with the three linear coefficients fixed. In the wet-mass basis, the coefficients multiply wet-mass fractions x_i; in the VS basis, they multiply volatile-solids fractions z_i. The inert-vegetable rows are bounding cases without bootstrap intervals because they are determined by the T1 and T3 means alone.

Figure 5a makes the structural limitation of the design visible: the four compositions occupy three edges and one interior point of the simplex, and no vertex was tested. Hence, the model only permits a linear-order formulation, and the vegetable coefficient in Figure 5b represents an extrapolation toward an unvisited vertex. Nevertheless, the sign of this coefficient does not depend on the extrapolation: it is supported by the contrast between T1 and T3, both of which were experimentally tested, and the bootstrap interval does not cross zero in any of the 20,000 resamples. The defensible interpretation is that vegetables act as a net inhibitor within the tested range, not that their isolated yield is negative. On the VS basis, the magnitude of the coefficient is large because the vegetable fraction contributes little volatile solids: to lower the yield of T1 from 36.8 mL g^{-1} VS, that fruit alone would give to the observed 18.9 with a VS share of only 17%, each gram of vegetable VS must carry an effect several times larger than its own fermentable content. An effect of that size is not dilution; it is consistent with the vegetable fraction contributing something that acts on the fermentation of the other fractions, a point taken up in Section 4.2.

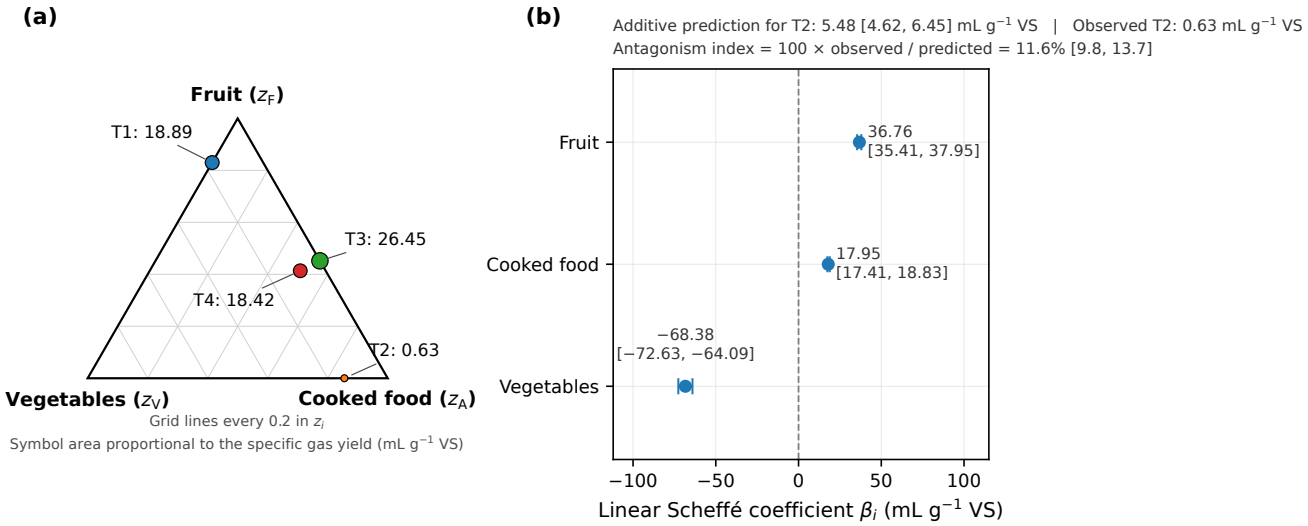

Figure 5. (**a**) Position of the four mixtures on the composition simplex expressed in volatile-solids fractions z_i (grid lines every 0.2), with symbol area proportional to the specific gas yield in mL g^{-1} VS, whose value is given next to each label; (**b**) linear Scheffé coefficients on the VS-fraction basis with 95% bootstrap confidence intervals based on 20,000 resamples, with the numerical values printed below each marker. The model is calibrated using the three fruit-containing mixtures and used to predict the fruit-free mixture, for which it yields 5.48 versus an observed value of 0.63 mL g^{-1} VS, corresponding to an antagonism index of 11.6% with a 95% confidence interval of 9.8% to 13.7%.

3.6. Screening of the Photofermentative Stage

The photofermentative stage produced 11.3 ± 0.6, 13.0 ± 1.7, and 20.7 ± 1.5 mL per liter of working volume (diluted effluent) at 2500, 3000, and 3500 lx over 96 h, respectively. The best condition corresponds to 0.38% of the volume obtained per kilogram in the dark-fermentation stage from the same substrate, or to about 1.1% after correcting for the 1:2 dilution of the effluent. The stage did not make a measurable contribution to the process and is therefore reported as a negative result; the probable causes are examined in Section 4.6. Because the light supply was characterized photometrically and without a recorded source spectrum, these values are not comparable with published photofermentation yields and are not used in any subsequent calculation.

3.7. Hydrogen Yield Bounds, Stoichiometric Closure, and Fate of the Residual Carbon and Energy

The hydrogen yield bounds and the closure relative to Equation (5) were determined for all experimental mixtures. Among the evaluated conditions, mixture T3 exhibited the best performance, the estimated specific hydrogen yield ranges from 11.90 mL H_2 g^{-1} VS in the reference case to 26.45 in the upper bound, corresponding to 4.37% and 9.71% of the maximum yield of the acetate pathway, respectively. At the stoichiometric bound of 66.7% v/v H_2, the highest physically consistent case, the yield is 17.63 mL H_2 g^{-1} VS, and the closure is 6.47%. Energy recovery is 0.76% and 1.68% of the chemical energy of the substrate. A methanogenic pathway applied to the same mixture would recover 73.8% with a biochemical methane potential of 350 L kg^{-1} VS and 84.3% with 400 L kg^{-1} VS, approximately two orders of magnitude more of the available energy. Propagating the assumed analytical uncertainties of the single-substrate determinations gives a 95% interval of 8.7% to 11.0% for the upper-bound closure of T3 and of 3.9% to 4.9% for the reference case, so the statement that no mixture reaches one-tenth of the stoichiometric ceiling holds at the limit of that interval and is reinforced, not weakened, by the uncorrected gas temperature.

The relevant feature of Table 9 is not the ranking but the scale. None of the mixtures exceeds 10% of the stoichiometric ceiling even under the most favorable assumption, in which all of the measured gas is hydrogen. Moreover, the ordering of the closure does not

reproduce that of the carbohydrate content: T2 contains more carbohydrates per kilogram than T1 and yet achieves a closure 30 times lower, confirming from the mass balance what the kinetics had already shown. The energy recovery column translates this closure into the magnitude relevant to a utilization decision: below 1% in the reference case, compared with 73.8–84.3% for the methanogenic pathway.

Table 9. Hydrogen yield bounds, stoichiometric closure, and energy recovery for the four mixtures.

Mixture	$V_{H_2}^{max}$ (mL kg^{-1})	Measured Gas (mL kg^{-1})	H_2 Yield		Closure		Energy Recovery
			RC	UB	RC	UB	RC
T1	34,874	2569	8.50	18.89	3.31	7.37	0.54
T2	43,753	110	0.29	0.63	0.11	0.25	0.02
T3	56,342	5469	11.90	26.45	4.37	9.71	0.76
T4	45,776	3210	8.29	18.41	3.16	7.01	0.53

Mixture coding according to Table 4. RC, reference case at 45% v/v H_2; UB, upper bound assuming that the entire gas phase consists of H_2. The carbohydrate contents used in Equation (5) are 70.08, 87.92, 113.22, and 91.99 g kg^{-1} for T1 to T4, respectively, derived from Table 4. Hydrogen yields are given in mL H_2 g^{-1} VS; closure is expressed as % of the stoichiometric maximum from Equation (5); energy recovery is expressed as % of a substrate chemical energy content of 17 MJ kg^{-1} VS. Values at the stoichiometric bound (66.7% v/v H_2) are two-thirds of the UB column.

Figure 6 traces where the carbon and the energy that did not leave as hydrogen went, for the T3 mixture and for the four combinations of gas composition (RC and SB) and pathway (acetate and butyrate). The carbon partition in Figure 6a,b is dominated by two blocks that the process did not touch: the unconverted carbohydrate carbon, 42.8% to 47.0% of the organic carbon of the mixture, and the carbon of the non-carbohydrate volatile solids, 50.8%. Carbon mineralized to CO_2 by the H_2-yielding pathway amounts to 0.72% to 2.12%, and the acids that accompany the hydrogen retain 1.43% to 4.24% in the effluent; in the reference case, the gas phase carries 0.32% to 1.03% of additional CO_2 that the H_2-yielding pathways cannot account for, and that must come from routes releasing CO_2 without hydrogen. Expressed relative to the carbohydrate pool alone, the hexose converted ranges from 4.37% (reference case, acetate) to 12.9% (stoichiometrically bound, butyrate), and between 95.7% and 98.5% of the carbohydrate carbon remains available to methanogens if the effluent is disposed of anaerobically. The energy partition in Figure 6c,d tells the same story in the units of a utilization decision: hydrogen carries 0.76% to 1.12% of the substrate energy, the volatile fatty acids in the effluent carry 1.2% to 4.6%, more than the hydrogen itself, and 98.8% to 99.2% of the chemical energy leaves the reactor in the effluent. The methanogenic reference recovers 73.8% to 84.3% of the same energy as methane. Two caveats apply to Figure 6a,b. The CO_2 that dissolved in the displacement water is not counted, so the mineralized carbon is somewhat larger than the gas-phase figures; and the partition assumes that all CO_2 produced along the H_2-yielding pathways reached the gas phase. Neither caveat affects the order of magnitude: if the collected gas had been entirely CO_2, it would have carried 2.93 g C kg^{-1}, 6.5% of the carbohydrate carbon, and even if the displacement water had absorbed as much CO_2 again, the carbon mineralized to the gas phase would remain below 13% of the carbohydrate carbon and below 7% of the estimated organic carbon of the mixture. The comparison does not argue against dark fermentation; it argues that, for this substrate, dark fermentation is an acidogenic first stage whose value lies in the effluent it produces, not in the gas.

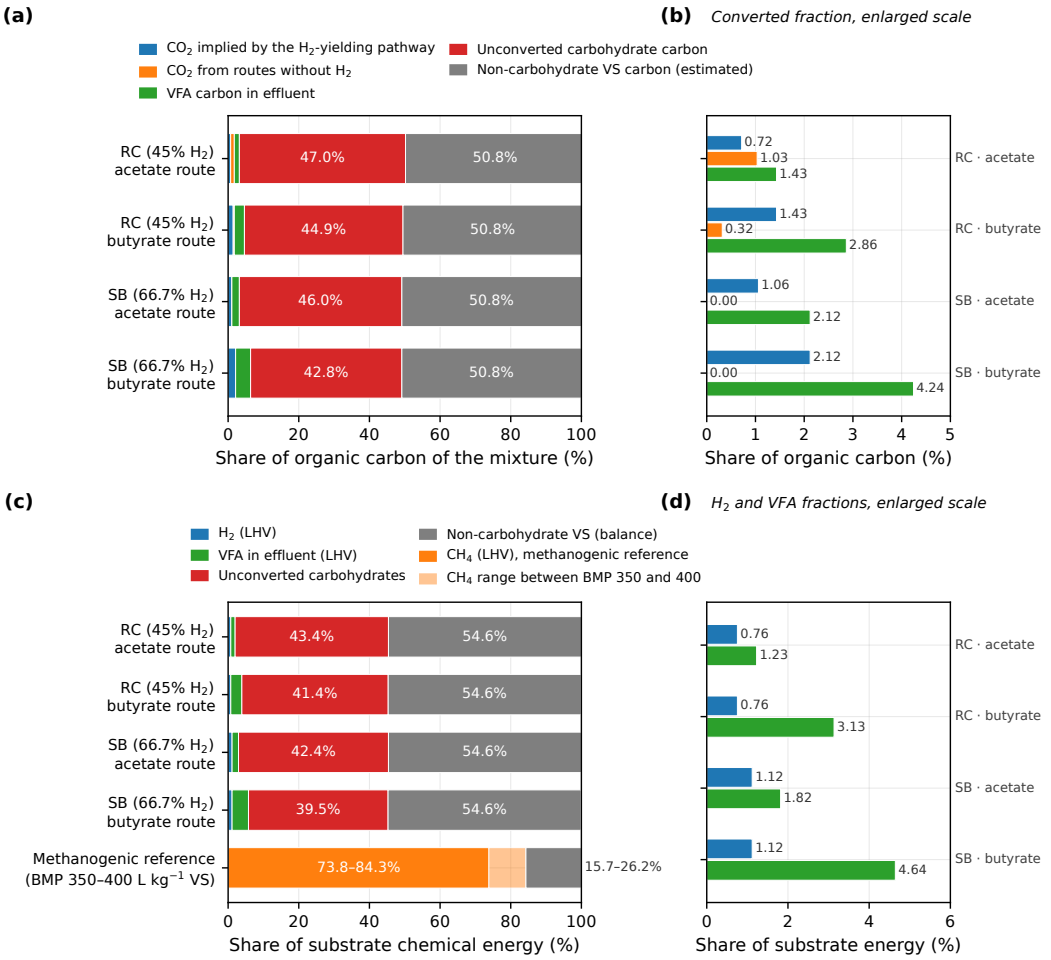

Figure 6. Fate of carbon and energy in the dark fermentation of the T3 mixture, per kilogram of wet mixture, for the reference case (RC, 45% v/v H_2) and the stoichiometric bound (SB, 66.7% v/v H_2), each evaluated for the acetate and the butyrate pathways: (**a**) partition of the organic carbon (measured carbohydrate carbon plus non-carbohydrate VS carbon estimated at 0.5 g C g^{-1} VS); (**b**) the converted fraction of (**a**) on an enlarged scale, with values in %; (**c**) partition of the substrate chemical energy (17 MJ kg^{-1} VS) on a lower-heating-value basis, with the methanogenic reference (BMP of 350–400 L CH_4 kg^{-1} VS) shown for comparison; (**d**) the H_2 and VFA fractions of (**c**) on an enlarged scale.

3.8. Corrected Climate Credit

For the T3 stream, which amounts to 582.4 kg $week^{-1}$ and is annualized to 30.28 t $year^{-1}$, Equation (6) yields 1.090 t CH_4 $year^{-1}$, corresponding to 30.53 t CO_2eq $year^{-1}$ under AR5 and 29.44 t CO_2eq $year^{-1}$ under AR6. With η_{H_2} ranging from 4.37% to 9.71%, the conversion-scaled credit from Equation (7) ranges from 1.29 to 2.86 t CO_2eq $year^{-1}$, meaning that the uncorrected figure overestimates the achievable benefit by a factor of 10 to 23, as shown in Figure 7b. The H_2-based factor is itself an upper bound: with the carbon-based factor of Equation (9), which ranges from 1.46% (reference case, acetate pathway) to 6.47% (upper bound, butyrate pathway), the credit falls to 0.43–1.90 t CO_2eq $year^{-1}$, and the overestimation factor rises to 15–69. At the stoichiometric bound, the two factors give 1.90 and 0.63–1.27 t CO_2eq $year^{-1}$, respectively. The carbon actually collected as CO_2 gives a third estimate that does not depend on the pathway: 3.6% of the carbohydrate carbon in the reference case, or 1.05 t CO_2eq $year^{-1}$. Whatever the composition, the carbon leaving in the collected gas cannot exceed 6.5% of the carbohydrate carbon, so the overestimation factor of the Tier-1 credit is at least 15 for any gas composition before the CO_2 dissolved in

the displacement water is considered, and at least 7 even if that dissolved CO_2 equaled the collected CO_2.

Two further qualifications concern the baseline rather than the conversion. First, the credit above refers to the T3 stream, which excludes the vegetable fraction and therefore presupposes stall-level separation; the stream that requires no separation is T4, 754.6 kg week^{-1} or 39.24 t year^{-1}, for which Equation (6) gives 1.413 t CH_4 year^{-1} and 38.14 t CO_2eq year^{-1} under AR6; with the T4 closure of 3.16% to 7.01%, the scaled credit is 1.20–2.67 t CO_2eq year^{-1} and the overestimation factor 14–32. Second, the conventional baseline uses two defaults that are generous for this substrate. Replacing MCF = 0.6 by the unmanaged-shallow value of 0.4 lowers the T3 baseline to 19.62 t CO_2eq year^{-1}; replacing the wet-basis DOC of 0.15 by the dry-basis default applied to the measured dry matter, 0.082, lowers it to 16.04; applying both gives 10.69. None of these alternatives changes the overestimation factor, which is the reciprocal of the conversion and independent of the baseline, but all of them show that the uncorrected credit of 29.44 t CO_2eq year^{-1} is inflated by a further factor of up to 2.8 before any conversion is considered.

The fossil fuel substitution term is even smaller. The annual hydrogen production of the T3 stream under the reference case is 74.5 m^3, corresponding to 6.7 kg or 804 MJ year^{-1}, equivalent to 223 kWh year^{-1}, which avoids between 45.1 kg CO_2 year^{-1} relative to natural gas, 59.6 kg CO_2 year^{-1} relative to diesel, and 76.1 kg CO_2 year^{-1} relative to bituminous coal. The two benefit terms therefore differ by more than one order of magnitude even after correction, and by almost three orders of magnitude before correction, so that any aggregated benefit claim is governed entirely by the assumption of avoided methane.

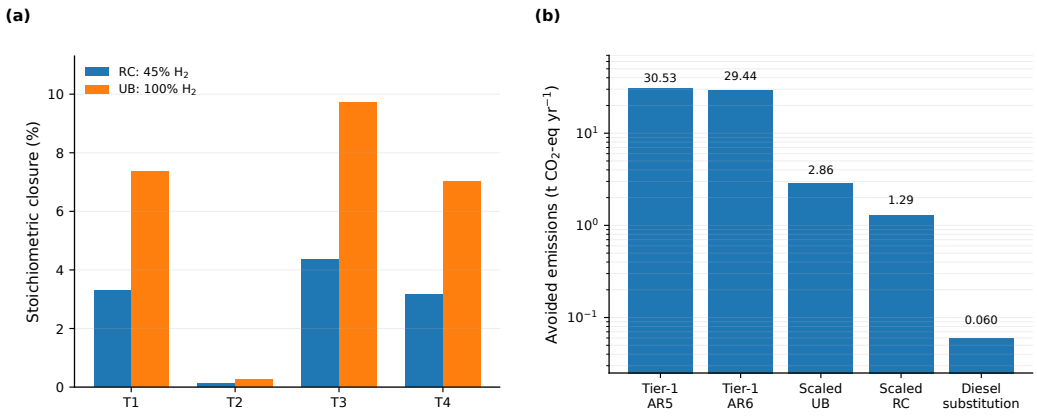

Figure 7. (**a**) Stoichiometric closure of each mixture relative to the maximum of the acetate pathway, for the two bounding assumptions regarding gas composition; (**b**) avoided emissions attributable to the T3 stream, comprising the uncorrected IPCC Tier-1 credit under the AR5 and AR6 metrics, the credit scaled by the H_2-based factor of Equation (7) under the upper-bound and reference cases, and the diesel substitution term. Note the logarithmic ordinate. RC, reference case at 45% v/v H_2; UB, upper bound with the entire gas phase assumed to be H_2.

The logarithmic ordinate in Figure 7b is a necessity rather than a graphical preference: the terms being compared span almost three orders of magnitude. When presented on a linear scale, the scaled credit and the fossil fuel substitution term would be indistinguishable from the axis, and this invisibility is precisely what allows an aggregated balance to be dominated by the uncorrected term without the reader noticing. The distance between the first two bars, only 3.7%, also shows that the choice between the AR5 and AR6 metrics is negligible compared with the correction for carbon conversion, which reduces the figure by more than one order of magnitude.

3.9. Uncertainty Propagation and Sensitivity of the Corrected Credit

The Monte Carlo simulation propagated the uncertainty of the seven parameters to the corrected credit; the results are presented in Table 10 and Figure 8. The proxy conversion factor based on the H_2 stoichiometric closure has a mean of 4.39%, with a 95% uncertainty interval from 3.25% to 5.75%, and the scaled credit is 1.32 t CO_2eq year^{-1}, with an interval from 0.84 to 1.99. The decisive point is that the overestimation factor does not approach unity in any of the 10,000 realizations: its 95% interval ranges from 17.4 to 30.8, and its minimum is 14.7, indicating that the conclusion does not depend on the point estimates selected for the accounting parameters.

Table 10. Monte Carlo uncertainty propagation for the T3 stream (N = 10,000, fixed seed, base prior $\mathcal{U}(0.35, 0.55)$ for the H_2 fraction).

Output Variable	Mean	95% UI Lower	95% UI Upper
η_{H_2} (%)	4.39	3.25	5.75
Uncorrected credit (t CO_2eq year^{-1})	30.04	21.63	40.41
Conversion-scaled credit (t CO_2eq year^{-1})	1.32	0.84	1.99
Overestimation factor	23.3	17.4	30.8

UI, empirical uncertainty interval defined by the 2.5th and 97.5th percentiles of the propagated distribution.

The Sobol decomposition, summarized in Table 11 and Figure 8c, provides the most incisive result of this section. The parameter contributing the greatest variance to the corrected credit is the volumetric hydrogen fraction, with a total index of 0.341, followed by the degradable fraction and the methane correction factor, each at 0.193. In other words, the largest individual source of uncertainty in the result is precisely the quantity that was not measured in the experiment. This quantifies the analytical cost of omitting gas chromatography: it is not a formal deficiency, but rather the term that governs the dispersion of the accounting conclusion.

It is also worth noting what the analysis rules out. The measured gas, which is the only experimental datum generated in this study that enters the balance, has a total index of 0.008 and is therefore practically irrelevant compared with the assumptions. The experimental precision achieved, with coefficients of variation between replicates ranging from 1.90% to 5.15%, comfortably exceeds what the remainder of the calculation chain can exploit. The sum of the first-order indices is 0.981, so interactions among parameters account for about 2% of the variance; this is the expected behavior of a product of independent factors with small dispersions, whose logarithm is additive, and it means that the parameters can be prioritized one at a time.

Table 11. First-order and total Sobol sensitivity indices for the conversion-scaled credit (D = 7, N_{base} = 16,384, N_{total} = 147,456, fixed seed), with 95% bootstrap confidence half-widths.

Parameter	S_i	S_{Ti}
H_2 fraction	0.330 ± 0.013	0.341 ± 0.008
DOC_F	0.186 ± 0.009	0.193 ± 0.005
MCF	0.186 ± 0.010	0.193 ± 0.005
Carbohydrates	0.134 ± 0.008	0.139 ± 0.004
DOC	0.119 ± 0.008	0.124 ± 0.003
GWP	0.020 ± 0.003	0.021 ± 0.001
Measured gas	0.007 ± 0.002	0.008 ± 0.000

Parameters with $S_{Ti} > 0.10$ are considered dominant. DOC, degradable organic carbon; DOC_F, fraction of DOC that decomposes; MCF, methane correction factor; GWP, global warming potential. Sum of first-order indices: 0.981.

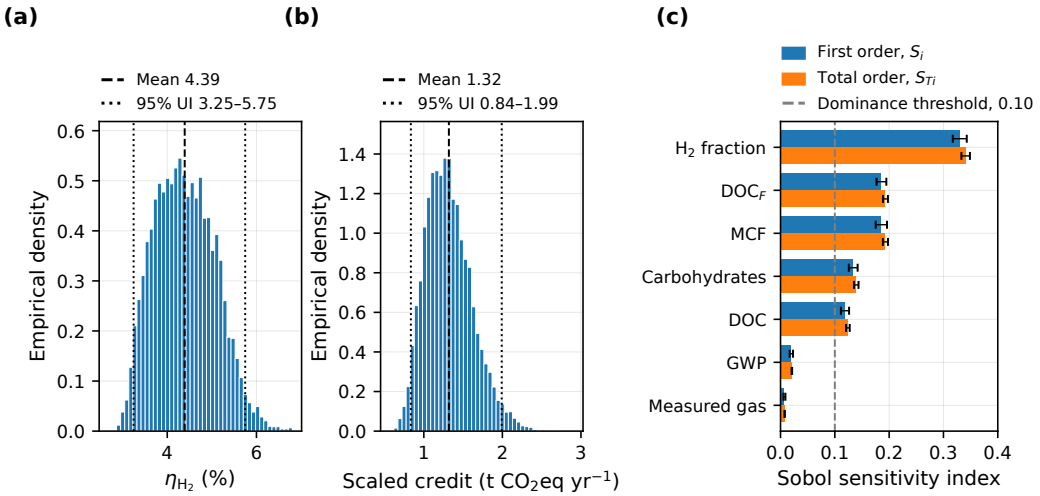

Figure 8. Uncertainty propagation and global sensitivity: (**a**) empirical distribution of the proxy conversion factor based on H_2 stoichiometric closure; (**b**) empirical distribution of the conversion-scaled credit; (**c**) first-order and total Sobol indices with 95% bootstrap confidence intervals, ordered by total index, with the dashed line indicating the dominance threshold of 0.10. In (**a**,**b**), the dashed line indicates the mean and the dotted lines the 2.5th and 97.5th percentiles from 10,000 realizations, with their values given above each panel.

The two distributions in Figure 8 are markedly right-skewed, which is a direct consequence of the model being a product of seven factors rather than a sum. This asymmetry has a practical implication: reporting only the mean overestimates the most probable value, and therefore the empirical interval in Table 10 is preferable to any expression of the form mean plus or minus standard deviation. Figure 8c, in turn, shows that the first-order and total indices differ only slightly for each parameter, confirming that interactions are small and are not concentrated in any particular parameter.

Table 12 and Figure 9 answer the question of how much the conclusion depends on the assumed range of gas composition. Narrowing the prior to $\mathcal{U}(0.40,\ 0.50)$ contracts the interval of the overestimation factor to 18.5–27.9; widening it to $\mathcal{U}(0.25,\ 0.667)$, whose upper limit is the stoichiometric maximum of the acetate pathway, expands it to 14.8–40.6 with a minimum of 12.2 across 10,000 realizations. The analytical sweep in Figure 9 extends the result to any fixed composition: the H_2-based factor is $V_{H_2}^{\max}/(f\,G)$, so it falls from 34.3 at 30% v/v H_2 to 15.5 at the stoichiometric bound and to 10.3 in the mathematical envelope of 100% H_2, and the carbon-based factor stays between 15 and 69 over the same range. There is no admissible gas composition for which the Tier-1 credit is justified, which is why the absence of gas chromatography limits the precision of the correction but not its direction.

Table 12. Sensitivity of the Monte Carlo results to the prior adopted for the volumetric H_2 fraction ($N = 10{,}000$ each, fixed seed, all other priors as in Section 2.12).

Prior for H_2 Fraction	η_{H_2} (%), 95% UI	Scaled Credit (t CO_2eq $Year^{-1}$), 95% UI	Overestimation Factor, 95% UI	Minimum Factor
Narrow, $\mathcal{U}(0.40,\ 0.50)$	3.58–5.39	0.89–1.89	18.5–27.9	15.9
Base, $\mathcal{U}(0.35,\ 0.55)$	3.25–5.75	0.84–1.99	17.4–30.8	14.7
Wide, $\mathcal{U}(0.25,\ 0.667)$	2.46–6.75	0.67–2.30	14.8–40.6	12.2

UI, empirical uncertainty interval (2.5–97.5th percentiles). The minimum factor is the smallest value observed among the 10,000 realizations.

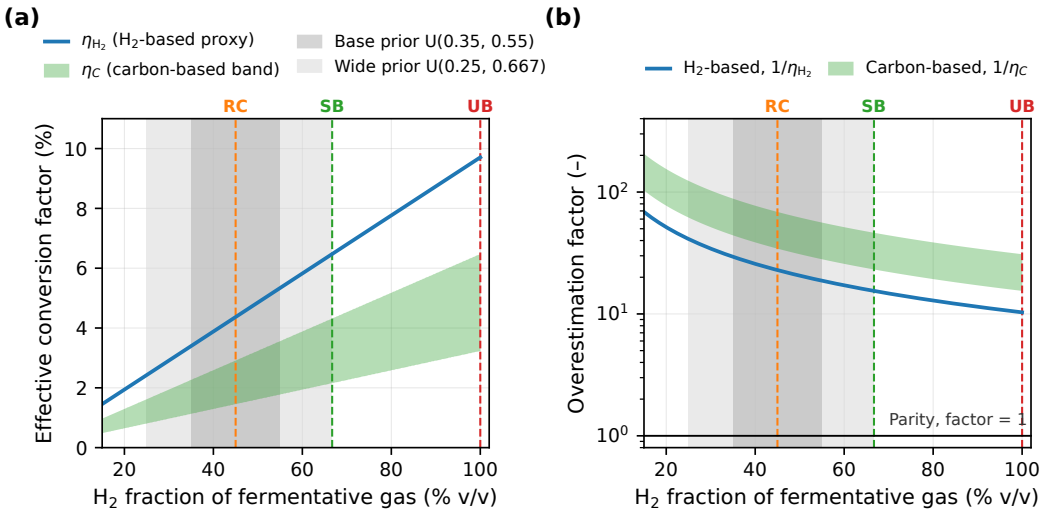

Figure 9. Dependence of the correction on the volumetric H_2 fraction of the fermentative gas for the T3 stream: (**a**) H_2-based conversion factor η_{H_2} and carbon-based factor η_C (band between the acetate and butyrate pathways); (**b**) overestimation factor of the Tier-1 credit on a logarithmic ordinate. Dashed lines mark the reference case (RC), the stoichiometric bound of the acetate pathway (SB), and the mathematical upper bound (UB); shaded bands mark the base and wide Monte Carlo priors of Table 12. The horizontal line at unity in (**b**) is the parity at which the uncorrected credit would be fully justified.

4. Discussion

4.1. Fruit Fraction as the Kinetic Driver of Acidogenesis

Across the composition simplex, the fruit fraction dominates the response. Its Scheffé coefficient is approximately twice that of cooked food, and its removal not only reduces the yield but also suppresses fermentation. Two properties of fruit waste are jointly consistent with this role: a carbohydrate pool dominated by directly fermentable mono- and disaccharides, which does not require a hydrolysis step, and an intrinsically acidic, weakly buffered character that, once the initial adjustment to pH 5.5 is made and in the absence of subsequent pH control, lets the medium acidify rapidly, which constitutes the only mechanism restricting hydrogen consumers in an uninoculated system [9]. The immediate onset of gas evolution in all mixtures containing fruit is the signature of a rapidly available soluble substrate rather than one limited by hydrolysis. Neither property was measured in this study; both are inferred from the composition of the fractions and from the shape of the curves, and the terminology adopted in the title, fruit-fraction-dependent rather than fruit-fraction-governed, reflects that the dependence is established empirically while the mechanism is not.

Cooked-food waste contributes approximately half as much per unit of volatile solids despite having the highest carbohydrate concentration among the three fractions (529.36 mg g^{-1} DM). This is consistent with a carbohydrate pool dominated by gelatinized starch, whose conversion is limited by hydrolysis over a 72 h timescale, and with a higher protein content whose degradation releases ammonia and increases the buffering capacity of the medium [11].

4.2. Mechanistic Hypotheses for the Collapse in the Absence of Fruit

The 88.4% suppression observed in the fruit-free mixture is reproducible across five independent reactors, with a coefficient of variation of 4.6%, indicating that it is a treatment-level phenomenon rather than a failed replicate. Substrate concentration does not explain it, since T2 provides more volatile solids per kilogram than T1 and a comparable carbohy-

drate concentration. Three hypotheses are consistent with the available data and are not mutually exclusive.

The first, and in our opinion the most likely, is a shift toward a fermentative pathway without gas generation. Food waste carries an indigenous microbiota dominated by lactobacilli that displaces *Clostridium* and collapses hydrogen production [13,14], homofermentative hexose fermentation yields lactate without gas evolution [10,12], and specifically in fruit and vegetable waste, pH and organic loading determine whether the pathway shifts toward lactate or hydrogen [21,52]. Two features of the fruit-free mixture favor this outcome: the vegetable and cooked-food fractions carry a high native load of lactic acid bacteria, the same organisms that drive the spontaneous fermentation of vegetables and cooked starch, and the higher protein content and buffering capacity of that matrix remove the rapid acidification with which fruit-derived sugars are fermented. All reactors started at the same adjusted pH of 5.5, so the difference cannot lie in the initial pH; it can lie in the trajectory that follows, which was not measured. The hypothesis therefore rests on the buffering capacity and on the microbial inoculum that each fraction contributes, not on an observed pH trajectory. This is also why lactic fermentation is deliberately used as a storage method prior to dark fermentation [53], and why configurations have been developed that reassimilate lactate using specific consuming bacteria [54–56]. This mechanism would produce exactly what was observed, namely substrate consumption without volume generation. The second hypothesis is early inhibition of the hydrogen-producing consortium by ammonia released from the protein fraction of cooked food and vegetable waste, aggravated by the absence of a low initial pH that would restrict proteolysis [11]. The third is hydrogen consumption by homoacetogens and hydrogenotrophic methanogens, which are not suppressed at near-neutral pH in the absence of thermal or acid pretreatment of the indigenous inoculum [32]. This mechanism is not excluded by the gas-volume data: homoacetogenesis consumes 4 mol H_2 and 2 mol CO_2 per mol of acetate formed and therefore removes gas volume entirely, and hydrogenotrophic methanogenesis converts 5 mol of gas into 1, so that complete consumption of the hydrogen from the acetate pathway would leave only one third of the volume. What limits the third hypothesis is kinetics rather than stoichiometry: without an acclimated inoculum, hydrogenotrophic methanogens grow too slowly to consume within 72 h the hydrogen that fruit-containing mixtures released from the first six hours onward, whereas homoacetogens are faster and cannot be discarded.

Table 13 confronts each hypothesis with the seven observations that the present dataset does establish. None of the three is contradicted by the gas-volume data alone, which is why the mechanism cannot be resolved; but the observations are not equally informative for each. The reproducibility of the collapse across five reactors (O2) and its occurrence on a substrate that is, by volatile solids, 86% cooked food (O3, O5) weigh against an explanation based on the intrinsic recalcitrance of any single fraction and in favor of an interaction carried by the vegetable fraction, either as inoculum (hypothesis 1) or as a nitrogen source (hypothesis 2). The immediate onset of gas in every fruit-containing reactor (O4), including T1 where vegetables are present, shows that vegetables do not suppress fermentation when fruit-derived sugars and acidity are available, which is compatible with hypotheses 1 and 2 and neutral for hypothesis 3. The absence of any detectable lag in T2 (O1) is the observation most at odds with hypothesis 3, because hydrogen consumption by a slow-growing population would be expected to allow an initial burst of gas that is later consumed, and no such burst was recorded at 6 h.

Table 13. Consistency of the three mechanistic hypotheses for the collapse of the fruit-free mixture with the observations established in this study, and the liquid-phase measurements that would discriminate between them.

Observation	H1: Homolactic Shift	H2: Ammonia Inhibition	H3: H_2 Consumption
O1. Near-zero gas at every reading from 6 h to 72 h, no initial burst	Consistent	Consistent	Weakly contradicted (a consumed burst would be expected)
O2. Collapse reproducible in five reactors, CV 4.6%	Consistent	Consistent	Consistent
O3. T2 supplies more VS and comparable carbohydrates per kg than T1	Consistent (substrate is not limiting)	Consistent	Consistent
O4. Immediate onset in every fruit-containing mixture, including T1 with vegetables	Consistent (fruit sugars and rapid acidification pre-empt lactic dominance)	Consistent (rapid acidification restricts proteolysis; all reactors started at pH 5.5)	Neutral
O5. Cooked food ferments readily with fruit (T3 highest yield)	Consistent	Consistent	Consistent
O6. Vegetable coefficient large and negative per gram of VS	Consistent (vegetables as LAB inoculum)	Consistent (vegetables as nitrogen source)	Neutral
O7. Photofermentation effluent of T3 evolved almost no further gas	Neutral	Neutral	Neutral
Discriminating measurements	Lactate accumulation; pH falling to 3.5–4.5; low acetate/butyrate	Total ammonia nitrogen above inhibitory thresholds; pH near neutral; VFAs present	Acetate without H_2 or CH_4 in headspace (homoacetogenesis); CH_4 in headspace (methanogenesis)

LAB, lactic acid bacteria; VFAs, volatile fatty acids. The hypotheses are not mutually exclusive; the last row lists the signature that would identify each as dominant.

Discriminating between these hypotheses requires speciation of the liquid phase into lactate, acetate, butyrate, propionate, and ethanol, together with a pH profile, total ammonia nitrogen, and the composition of the headspace, none of which is available for this dataset. The hypotheses are therefore presented as such, and the experimental design required to resolve them is specified in Section 4.9. What the present data establish is more limited but robust: within a market-waste stream, the presence of a fruit fraction is a necessary condition for acidogenic gas production over a 72 h timescale, and its absence cannot be compensated for by increasing the loading of the remaining fractions.

4.3. The Normalization Basis Is Not a Formality

The change in the rankings on a wet-mass basis and on a volatile-solids basis between T1 and T4 constitutes a methodological result in its own right. Mixtures formulated to reproduce waste-generation ratios necessarily differ in moisture content, here by 6.6 percentage points across the dataset, and a yield expressed on a wet-mass basis therefore incorporates a water-content term. Reporting mL kg^{-1} of wet mixture, as is common in applied screening studies, would have led to selecting the ternary mixture as the best three-component formulation, a conclusion that is not supported by the volatile-solids-normalized analysis, with $p = 0.713$. When mixture compositions are dictated by a waste stream rather than by a simplex design, normalization per gram of volatile solids is not optional; the same rationale underlies the normalization conventions of standardized biochemical methane potential protocols [39,40]. The same logic applies to the additivity test itself: an additive expectation formulated on wet-mass fractions for a VS-normalized response mixes two bases, which is why the primary mixture model of this revised analysis is formulated on volatile-solids fractions, and the wet-mass version is retained only as a sensitivity case (Table 8).

4.4. Positioning Against the Recent State of the Art and Scope of Novelty

The relevant comparison is not with the general biohydrogen literature, but with recent studies employing real food waste, waste mixtures, lactate-driven pathways, two-stage systems, or environmental assessments. Tables 14 and 15 summarize this positioning. The emerging pattern is clear: the recent literature has improved process operation through pH, solids, loading, inoculation, pretreatment, stage separation, and continuous operation control, whereas this study addresses a different question: whether the response of a real-world mixture can be treated as additive and whether the climate benefit attributed to waste diversion is compatible with the degree of conversion that the experiment itself can substantiate.

Table 14. Positioning of the present study relative to recent studies on dark fermentation of food waste and waste mixtures (Part I).

Study	Substrate/System	Main Question	Difference from the Present Work
Martínez-Mendoza et al. [21]	Fruit and vegetable waste; lactate-driven fermentation	Effect of operational parameters on H_2 production	Addresses operational control and metabolic pathway; does not test the additivity of mixtures inherited from a real waste stream.
Regueira-Marcos et al. [22]	Food waste	Effect of pH and total solids on H_2 and carboxylic acid production	Manipulates process variables; does not use an excluded composition to test an additive expectation.
Regueira-Marcos et al. [24]	Restaurant waste; continuous operation	Robustness to HRT and feast/famine disturbances	Evaluates the dynamic stability of a composite substrate; does not statistically decompose the contribution of individual fractions.
Roslan et al. [53]	Food waste	Lactic fermentation as a storage strategy prior to DF	Converts lactate production into a deliberate conditioning strategy; here, the focus is on diagnosing the spontaneous collapse of a fruit-free mixture.
Perat et al. [27]	Waste mixtures	Mixing interactions and the role of H_2-producing/consuming communities	Provides the closest conceptual precedent on mixture interactions; the present work adds a formal Scheffé additive expectation, out-of-calibration prediction, and a bootstrap-based antagonism index.
Vázquez-López and Moreno-Andrade [28]	Food waste + corn-industry wastewater	Co-digestion to improve balance, alkalinity, and organic loading	Uses mixing as a process-improvement strategy; here, the mixture reproduces proportions observed in the market and is tested for additive behavior.
Villanueva-Galindo et al. [54]	Lactate-rich effluent from food-waste treatment	Effect of lactate-consuming bacteria on H_2	Provides microbiological resolution of the lactate pathway; in this work, that pathway is proposed as a mechanistic hypothesis rather than a directly measured mechanism.

The preceding comparison makes it possible to distinguish technological novelty from methodological novelty. This work does not propose a new metabolic pathway, a new microorganism, or a reactor with higher productivity. Its contribution lies in introducing three consistency checks that rarely appear together. The first is compositional: the proportions are not selected to maximize H_2, but are inherited from the observed waste stream. The second is statistical: one composition is excluded from the calibration and used as an external validation of the additive expectation, so that the deviation can be quantified as

antagonism rather than merely described as a difference between treatments. The third is physical-accounting based: the yield is compared with a stoichiometric ceiling before being translated into a climate benefit. This sequence reduces the possibility that a favorable conclusion depends on the normalization basis, on an unverified mixture interaction, or on crediting as avoided carbon that remains in the residual stream.

Table 15. Positioning of the present study relative to recent studies on dark fermentation, scale-up, and environmental assessment (Part II).

Study	Substrate/System	Main Question	Difference from the Present Work
Martínez-Fraile et al. [55]	Real organic waste from treatment plants	H_2 production by lactate-driven dark fermentation	Demonstrates transferability to real waste; does not examine non-additivity of fractions or dependence on the normalization basis.
Regueira-Marcos et al. [25]	Food waste; continuous two-stage system	Physical separation of lactate and H_2 production	Optimizes bioprocess architecture; here, the second stage is used as a screening step, with the focus on composition–conversion–accounting traceability.
Kim and Cho [57]	Food waste; thermophilic fermentation	Synergy and bacterial relay in H_2 production	Resolves microbial interactions through a thermophilic strategy; does not address a mixture additivity test or climate credit.
Das and Basak [58]	Potato waste; dark fermentation and photofermentation	Optimization of substrate concentration and sequential production	Optimizes a defined feedstock; the present study works with real heterogeneity imposed by the waste stream.
Gbiete et al. [59]	Restaurant waste	Comprehensive characterization oriented toward DF scale-up	Reinforces the need to characterize real substrates; here, that characterization is linked to a mixture-interaction test and a stoichiometric closure.
Lee et al. [29]	Dark fermentation of food waste followed by anaerobic digestion	GHG emissions and net energy production	Quantifies the environmental performance of an integrated configuration; the present work questions an earlier stage of the accounting: how much avoided-methane credit can be attributed when acidogenic conversion is incomplete.
Jin et al. [30]	Wheat straw; dark–photo fermentation	LCA of an integrated biohydrogen pathway	Assesses life-cycle impacts of a complete pathway; here, the physical consistency between measured conversion and baseline credit is analyzed before conducting a full LCA.
Zhang et al. [31]	Pilot-scale dark fermentation and photofermentation systems	Commercial feasibility, energy, emissions, and payback period	Extends the discussion to pilot scale; the present study provides a substrate-scale and accounting consistency test that should precede scale-up.

The closest antecedent to the mixture contribution is Perat et al. [27], because it demonstrates that mixing waste alters the fermentative ecology and can change the net H_2 production. The methodological difference is important: whereas that approach investigates the mechanisms and consequences of mixing, here, an additive counterfactual prediction is constructed from the fruit-containing mixtures and tested against a composition not used in the calibration. The result of 0.63 versus 5.48 mL g^{-1} VS does not simply mean that T2 is "worse"; it means that it produces only 11.6% of what an additive model would have expected for its composition, and between 2.5% and 13.7% of what any admissible additive model would have expected. This formulation makes antagonism comparable

across future studies even when the fractions or absolute production units change. The advance over the existing literature is therefore not the observation that fruit-rich waste ferments better, which is well known, but the demonstration, with a bounded index, that a real fruit-free mixture behaves as a suppressed system rather than as a diluted one, and the identification of the fruit fraction as a necessary condition whose absence cannot be compensated by loading.

The comparison with Lee et al. [29], Jin et al. [30], and Zhang et al. [31] similarly delineates the environmental contribution. These studies advance toward energy balances, LCA, and system-scale sustainability, whereas the present study is situated one logical level earlier: it verifies whether the magnitude of the benefit attributed to waste diversion is compatible with the conversion observed in the acidogenic stage. In this sense, the contribution does not replace an LCA; rather, it functions as a consistency condition to prevent a potential baseline from being automatically converted into a process credit.

A critical terminological distinction must nevertheless be maintained. The ratio $V_{H_2}^{meas}/V_{H_2}^{max}$ is a stoichiometric-closure proxy based on H_2; it is not a direct measurement of carbon mineralization, because H_2 contains no carbon and substrate carbon may remain in acetate, butyrate, lactate, biomass, dissolved CO_2, or other products. Equation (9) and Figure 6 make this explicit: the carbon-based factor is one-third to two-thirds of the H_2-based proxy, and the interval of 1.29–2.86 t CO_2eq yr^{-1} should be read as an upper bound whose carbon-consistent counterpart is 0.43–1.90 t CO_2eq yr^{-1}. This qualification strengthens rather than weakens the main conclusion: with the available data, there is no physical basis for automatically assigning the full Tier-1 credit of the diverted mass to an acidogenic stage that leaves most of the carbon in the effluent. The subsequent fate of that carbon remains the necessary variable for closing the net mitigation balance.

4.5. Scope of the Kinetic Model and the Structured-Model Route

The modified Gompertz equation is used in this study as a descriptive summary of the measured curves, and no mechanistic claim is derived from its parameters: the only inference drawn from the fit is that the assay reached its asymptote, which is verified directly against the measured 72 h yields, and the differences among mixtures are established on the measured yields with heteroscedastic tests. The stronger statements of the study, namely the non-additivity of the response and the stoichiometric ceiling, do not use the Gompertz parameters at all.

A structured model such as the Anaerobic Digestion Model No. 1 [60] in the variants extended to fermentative hydrogen production [61,62] would indeed be the appropriate route to a mechanistic interpretation, and it is the modeling stage planned for the confirmatory campaign of Section 4.9. It cannot be applied to the present dataset for a reason of identifiability rather than of preference. ADM1-based descriptions of dark fermentation resolve at least sugar uptake, biomass growth, the partition of hexose among acetate, butyrate, lactate, propionate and ethanol, hydrogen inhibition, and the acid–base and gas–liquid equilibria that set pH and headspace composition; even the reduced formulation of Gadhamshetty et al. [62] was calibrated against measured hydrogen, chemical oxygen demand and volatile fatty acids. The present experiment recorded a single state variable, cumulative gas volume, at 12 points per reactor. Calibrating a model with more than 10 kinetic and stoichiometric parameters to 12 observations of one aggregated output would return parameter sets that reproduce the curve without being identifiable, and any mechanistic conclusion drawn from them would be an artifact of the regularization chosen. The three-parameter Gompertz form is, in that sense, the most complex model the data can support, and its use is a consequence of the same limitation that prevents the mechanistic resolution of the fruit-free collapse. Once the liquid-phase speciation, the pH trajectory,

and the headspace composition of the confirmatory campaign are available, an ADM1-based model with variable stoichiometry [61] becomes identifiable, and the hypotheses of Section 4.2 can be tested as alternative model structures rather than as verbal alternatives.

4.6. Why the Two-Stage Pathway Did Not Perform

The photofermentative stage contributed 0.378% of the production of the dark fermentation stage, although the residual volatile fatty acids in the effluent should, in principle, contain most of the remaining hydrogen potential [15,16]. Three features of the design explain this result, and all three are correctable.

First, and most fundamentally, the light supply was specified in lux. Illuminance is a photometric quantity weighted by the human photopic response, which peaks at 555 nm and is practically negligible beyond 750 nm. The light-harvesting complexes of purple non-sulfur bacteria absorb approximately at 522, 590, and 800–860 nm, so illuminance provides practically no information about the radiation driving photofermentation [17,18]. The appropriate specification is irradiance in W m^{-2} over 400–950 nm, with the source spectrum reported; on that basis, the three nominal levels used here may not have differed materially at all. Because the source spectrum was not recorded, no conversion of the illuminance values to irradiance is possible, and the stage is not comparable with any study reporting radiometric quantities; this is why it is reported as a screening result and excluded from every calculation. Second, no purple non-sulfur bacterial inoculum was added; the effluent was filtered and diluted 1:2, which lowered the concentration of volatile fatty acids and the turbidity, but without an inoculum, the catalytic capacity of the stage was never established. Third, temperature was not controlled, whereas the relevant mesophilic optimum is 30–35 °C. The stage is reported as a negative result because the reasons for the negative outcome are instructive: they are the same factors that make two-stage yields published at field scale difficult to reproduce.

4.7. Implications for Avoided-Methane Accounting

The central accounting result is general and does not depend on the specific yields measured here. The IPCC default equation estimates the potential methane that a given mass of waste would generate at a disposal site, without considering the timing of the emission, and the guidelines themselves caution that its results are not comparable with those of the first-order decay model [19,20]. Twenty years of application of the protocol have documented that the mass-balance method systematically overestimates annual emissions and that its use outside national inventories requires these limitations to be made explicit [35]. Crediting the full amount to a diversion scheme is legitimate only if the scheme destroys the degradable organic carbon. Anaerobic digestion to methane approaches this condition; acidogenic fermentation does not. With a closure of 4.37% to 9.71% relative to the carbohydrate pool alone, and with that pool itself representing only part of the degradable organic carbon, the effluent leaves the process carrying the overwhelming majority of that carbon; Figure 6 puts the figure at 95.7% to 98.5% of the carbohydrate carbon and at more than 98% of the substrate energy. If the effluent is discharged untreated, practically the entire baseline emission is shifted in time rather than avoided.

Equation (7) constitutes a minimum correction: it scales the credit using a conversion proxy factor based on the stoichiometric closure of H_2. Applied here, it reduces the claim from 29.44 to an interval of 1.29–2.86 t CO_2eq yr^{-1}, and the carbon-consistent factor of Equation (9) reduces it further to 0.43–1.90 t CO_2eq yr^{-1}. A more complete accounting should additionally incorporate the energy demand of the process, namely continuous lighting for 96 h in the photofermentative stage, agitation, and any thermal conditioning, which, for the measured production of the illuminated stage, exceeds the energy produced

by several orders of magnitude. The practical conclusion is that dark fermentation of market waste should be presented as a first acidogenic stage within a cascade that ends in methanogenesis or composting, rather than as an autonomous climate mitigation measure. Crediting the standalone configuration with the full Tier-1 term is the largest individual source of overestimation identified in this work.

Two additional accounting observations deserve mention. The default mass-balance equation used here was superseded by the first-order decay model in the 2006 IPCC Guidelines [20], and its continued use in applied studies should be justified rather than assumed [35]. The choice of global warming potential matters much less than the conversion-based scaling, but AR6 should nevertheless be followed, with a value of 27 for non-fossil methane, rather than AR5 [45].

For practitioners who prepare the environmental accounting of small-scale organic-waste hydrogen projects, the results translate into six operational recommendations. First, the diverted mass is the input to the baseline, never the credit: the baseline of Equation (6) should be computed and reported, but the credit claimed should be the baseline multiplied by a conversion factor demonstrated for the project. Second, the conversion factor should be carbon-based: for dark fermentation, it is the fraction of the degradable carbon that the project mineralizes to CO_2 or captures as methane and oxidizes, obtained from measured gas composition and a liquid-phase carbon balance; the H_2-based proxy of Equation (8) may be used only as an upper bound when no liquid-phase data exist, and it should then be labelled as such. Third, the fate of the effluent must be declared and accounted: an effluent sent to anaerobic digestion or aerobic composting earns the credit of that second stage, whereas an effluent discharged or landfilled earns none and returns most of the baseline emission. Fourth, when the gas composition has not been measured, the credit should be reported as an interval spanning the admissible compositions, as in Table 12, rather than as a point value, and the interval should be accompanied by the sensitivity ranking of its inputs. Fifth, the baseline parameters should be adapted to the substrate: the wet-basis DOC default assumes a moisture content near 60%, and market waste with 80% moisture warrants the dry-basis default applied to measured dry matter; the methane correction factor should match the documented site category. Sixth, the conversion factor should be re-measured whenever the composition of the feed changes materially, because the response of a mixture is not additive: a stream that loses its fruit fraction can lose almost all of its gas production, and with it the entire basis of the credit. These recommendations mirror the tier structure of the IPCC inventories: a default proxy where nothing is measured, a measured gas composition where it is, and a closed carbon balance where the project claims the credit.

4.8. Limitations

The limitations of this dataset are substantial and are stated explicitly so that the conclusions can be weighted accordingly.

First, and critically for the interpretation of the results, the gas phase was not speciated. No chromatographic or sensor-based determination of its composition was performed. The measured response is cumulative fermentative gas, and all quantities referring to hydrogen are reported as a bounded interval between the reference case and the upper bound. No value from this work should be cited as a directly measured hydrogen yield. The suppression of the fruit-free mixture, by contrast, is a statement about total gas and does not depend on the composition assumption.

Second, no pH-trajectory or volatile fatty acid data are available; only the initial pH, adjusted to 5.5 in every reactor, is known. This prevents mechanistic resolution of the

collapse in the absence of fruit, which is therefore presented as a quantified phenomenon with candidate explanations rather than as an established mechanism.

Third, no inoculum blank was run. The yields are gross rather than net of endogenous gas production, which biases all absolute values upward by an unknown magnitude without affecting the ranking.

Fourth, only a single laboratory determination was performed for each fraction. The properties of the mixtures in Table 4 are propagated from three unreplicated analyses with no reported measurement uncertainty, and the parameters fall outside the laboratory's scope of accreditation. The phenol–sulfuric acid method quantifies soluble carbohydrates unless preceded by acid hydrolysis, a detail that the test report does not specify; if hydrolysis was not applied, the reported values underestimate the total carbohydrates of the cooked-food fraction, which is rich in starch, and the closure in Table 9 is correspondingly optimistic. The propagation of assumed analytical uncertainties in Section 3.7 bounds the effect of the missing replication on the closure at roughly $\pm$12% relative, and the antagonism index is algebraically independent of the VS determinations; neither result, however, can substitute for the replicated determinations of the confirmatory campaign.

Fifth, the generation census and the analytical campaign were conducted approximately eight months apart (September 2025 and May 2026), so the mass fractions of the mixtures and the properties of the fractions were not derived from the same material.

Sixth, the census covers a single week. Annualization to 52 weeks assumes the absence of seasonal variation and does not carry a confidence interval, while the observed weekend maximum within the census week suggests that intra-annual variability is unlikely to be negligible.

Seventh, the 6 h sampling interval does not resolve the lag phase, so the fitted negative values of λ are extrapolation artifacts rather than estimates.

Eighth, the dispersion among replicates of mixture T4 is anomalous. Its coefficient of variation at 72 h is 0.37%, compared with 1.90% to 5.15% for the remaining mixtures, an implausibly low value for biological quintuplicates measured with 5 mL resolution; the early measurements of the same mixture show the opposite pattern, with a coefficient of variation of 22% at 6 h (readings from 280 to 550 mL), which falls to 1.4% at 12 h and stays below 2% thereafter. The original reading sheets and the data log (Dataset S1) were re-examined during the revision of this article: the five series are distinct at every reading, monotonic, and recorded at the 5 mL resolution of the cylinder; no transcription error was identified, and the pattern is stated explicitly rather than corrected. Section 3.4 shows that the statistical conclusion for the T1–T4 pair is unchanged if the dispersion of T4 is inflated to that of the other mixtures, but the comparison between T1 and T4 should be considered provisional until remeasurement.

Ninth, two non-monotonic readings were corrected using a cumulative maximum envelope, with a documented effect of $+0.07$% on the mean of mixture T3.

Tenth, the mixture model is not identifiable at quadratic order. Only four compositions were tested and no fraction was fermented separately, so the vegetable coefficient is an extrapolation to a composition that was never experimentally tested. Its negative sign should be interpreted as indicating that the vegetable fraction acts as a net inhibitor within the range of compositions tested, rather than as a physical claim about vegetable waste in isolation. The single binary interaction that the four points can identify, β_{VA}, is reported in Table 8 as the size of the departure from linear blending, not as a validated higher-order model.

Eleventh, the gas volumes were recorded at laboratory conditions, and the temperature was not logged per reactor, so the volumes were not corrected to standard conditions; for the 18–25 °C range recorded in the laboratory, the closure values are overestimated by 6–13%, in

the direction that strengthens the conclusions. Twelfth, the displacement liquid was water, so part of the CO_2 dissolved during collection; the hydrogen upper bound is unaffected, but the total gas and the mineralized carbon are underestimated by an amount that was not measured and that the composition-independent bound of Section 3.8 accommodates.

4.9. Confirmatory Campaign and Research Route

The limitations above define the confirmatory campaign and the stages that follow it, summarized in Table 16. The confirmatory campaign is designed to answer four questions that the present dataset leaves open. The first is the actual hydrogen fraction of the gas, which the Sobol decomposition identifies as the dominant source of uncertainty in the credit; gas chromatography of the headspace at each sampling time converts the bounded intervals of this study into measured yields and, through the CO_2 balance, constrains the pathway partition. The second is the mechanism of the fruit-free collapse; the liquid-phase speciation of lactate, acetate, butyrate, propionate and ethanol, the pH trajectory and the total ammonia nitrogen provide the discriminating signatures of Table 13. The third is the identification of the quadratic Scheffé model; fermenting each fraction separately, in addition to the four mixtures, yields seven compositions and makes the three binary interaction terms estimable rather than inferred by exclusion. The fourth is the closure of the carbon balance; soluble COD, VFA carbon and headspace carbon allow the carbon-based factor of Equation (9) to be measured instead of bounded, which is the quantity that a credit ultimately requires. Nine reactors, three fractions in triplicate, are the minimum for the third question; the full campaign therefore repeats the four mixtures with the added instrumentation, in quintuplicate as before, and adds the three pure fractions, giving 35 reactors.

The stages that follow the campaign are sequenced by dependence. The carbon-balance stage closes the credit correction with measured quantities and specifies the fate matrix of the effluent for the two realistic second stages, anaerobic digestion and composting. The techno-economic assessment then evaluates the dark-fermentation–anaerobic-digestion cascade at the scale of the stream measured here, 30–40 t yr^{-1} for one market and its multiples for a district, with the effluent valued as digester feed rather than the hydrogen as fuel, since the energy balance of Figure 6 places the value in the effluent. The life-cycle assessment adopts the functional unit of 1 tonne of market waste managed, a baseline of uncontrolled disposal modeled with the first-order decay method rather than the mass-balance default, and system boundaries that include the second stage and the fate of the digestate, so that the avoided-methane term enters as a measured conversion and not as a diverted mass. The structured-model stage calibrates an ADM1-based description with variable stoichiometry on the campaign data and uses it to test the hypotheses of Section 4.2 as alternative model structures.

Table 16. Research route following the present study: questions, design, and measurements of the confirmatory campaign and of the subsequent stages.

Stage	Core Question	Design and Measurements
1. Confirmatory campaign	Q1: What is the H_2 fraction of the gas? Q2: Which mechanism suppresses the fruit-free mixture? Q3: Are the binary interactions of the mixture model estimable? Q4: How much carbon is mineralized?	Four mixtures in quintuplicate plus the three pure fractions in triplicate (35 reactors); headspace GC for H_2, CO_2 and CH_4 at each 6 h reading; pH trajectory; lactate, acetate, butyrate, propionate and ethanol; total ammonia nitrogen; soluble COD; C/N of each fraction; replicated substrate characterization; inoculum blank; gas volumes corrected to standard conditions; temperature logged; where feasible, 16S rRNA community profiling of the fractions and effluents

Table 16. *Cont.*

Stage	Core Question	Design and Measurements
2. Carbon-balance closure	What fraction of the degradable carbon does the process remove from the methanogenic pool, and where does the rest go?	Carbon balance across gas, acids and residual solids; measured η_C replacing Equation (9); fate matrix of the effluent under anaerobic digestion and composting
3. Techno-economic assessment	Is a decentralized dark-fermentation–anaerobic-digestion cascade viable at the scale of one market or a district?	Stream of 30–40 t yr^{-1} per market; effluent valued as digester feed; capital and operating costs of the two stages; sensitivity to gate fees and to the fruit share of the stream
4. Life-cycle assessment	What is the net mitigation per tonne of market waste managed?	Functional unit of one tonne managed; baseline of uncontrolled disposal with the first-order decay model; boundaries including the second stage and the digestate; avoided methane entered as measured conversion
5. Structured modeling	Can the mixture response and the collapse be reproduced mechanistically?	ADM1-based model with variable stoichiometry calibrated on Stage 1 data; hypotheses H1–H3 implemented as alternative structures and compared by identifiability and fit

GC, gas chromatography; COD, chemical oxygen demand.

5. Conclusions

The organic waste stream from El Pino market is dominated by fruit, which represents 41.04% of a total of 754.6 kg per week, followed by cooked food at 36.14% and vegetables at 22.82%.

Acidogenic gas production depends on the fruit fraction. The specific yields ranked F + A with 26.45 mL g^{-1} VS above F + V with 18.89 and F + V + A with 18.41, and well above V + A with 0.63, while the modified Gompertz model described all four mixtures with an R^2 of at least 0.982. The suppression of the fruit-free mixture, a factor of 41.7 (95% bootstrap interval 40.2–43.4) relative to F + A, refers to total fermentative gas and does not depend on any assumption about gas composition.

The fruit-free mixture produced 11.6% of the yield predicted by an additive mixture model formulated on volatile-solids fractions, with a 95% bootstrap confidence interval of 9.8% to 13.7%, and between 2.5% and 13.7% of the yield predicted by any admissible additive null. This 88.4% suppression cannot be explained by substrate concentration and identifies strong compositional antagonism in the mixture-design sense; the binary vegetable–cooked-food interaction required to reconcile the observation with linear blending, −39.2 mL g^{-1} VS, is of the same order as the main effects. The mechanism remains unresolved; the three candidate hypotheses are each consistent with the gas-volume data, and the liquid-phase measurements that discriminate between them are specified.

The normalization basis changes the conclusion. The ternary mixture is superior to F + V on a wet-basis basis and statistically indistinguishable from it per gram of added volatile solids, with $p = 0.713$. Normalization per gram of volatile solids is therefore mandatory whenever mixture compositions are determined by a waste stream, for the additivity test as much as for the ranking.

The estimated specific hydrogen yield of the best mixture is 11.90 to 26.45 mL H_2 g^{-1} VS, corresponding to 4.37% to 9.71% of the maximum yield of the acetate pathway, with an energy recovery of 0.76% to 1.68%. The carbon and energy balance shows that 95.7% to 98.5% of the carbohydrate carbon and more than 98% of the substrate energy leave the process in the effluent, so that dark fermentation of this substrate is an acidogenic first stage whose value lies in the effluent rather than in the gas. Acidogenic fermentation therefore leaves the vast majority of the degradable carbon in the effluent, and scaling the IPCC Tier-1 avoided-methane credit by the H_2-based proxy reduces it from 29.44 to an interval of

1.29 to 2.86 t CO_2eq yr^{-1}, while the pathway-consistent carbon-based factor reduces it to 0.43 to 1.90 t CO_2eq yr^{-1}; no admissible gas composition brings the overestimation factor below 10, and the Monte Carlo minimum across three priors for the hydrogen fraction is 12. Avoided-methane credits from dark fermentation should not be derived from the diverted mass alone; they must be conditioned on the conversion actually demonstrated and on the fate of the residual carbon. For practitioners, this means computing the baseline from the diverted mass but claiming only the baseline multiplied by a measured, carbon-based conversion factor, declaring the fate of the effluent, and reporting an interval rather than a point value whenever the gas composition has not been measured.

Two boundaries of the estimate deserve emphasis. The gas phase was not speciated, so all hydrogen values are bounded estimates rather than measurements, and the reported yields are the gross rather than net of endogenous gas production. Resolving both issues, discriminating among the mechanistic hypotheses, and identifying the binary interactions of the mixture model require the 35-reactor confirmatory campaign specified in Section 4.9, which, together with the carbon-balance closure, the techno-economic assessment of the dark-fermentation–anaerobic-digestion cascade, the life-cycle assessment with a first-order-decay baseline, and the ADM1-based structured modeling, defines the research route of this line.

Supplementary Materials: The following supporting information can be downloaded at https://www.mdpi.com/article/10.3390/hydrogen7040139/s1, Dataset S1, original and envelope-corrected cumulative gas readings for the 20 reactors (240 observations, CSV); Code S1, analysis script reproducing all statistical tests, bootstrap intervals, Monte Carlo propagation, and Sobol indices; Code S2, figure-generation script.

Author Contributions: Conceptualization, N.F.C.A., A.H.V., Y.C.A. and R.J.B.; methodology, Y.C.A. and R.J.B.; software, Y.C.A.; validation, N.F.C.A., A.H.V. and R.J.B.; formal analysis, Y.C.A. and R.J.B.; investigation, N.F.C.A. and A.H.V.; resources, N.F.C.A., A.H.V. and Y.C.A.; data curation, Y.C.A. and R.J.B.; writing—original draft preparation, Y.C.A., N.F.C.A. and A.H.V.; writing—review and editing, N.F.C.A., A.H.V., Y.C.A. and R.J.B.; visualization, Y.C.A. and R.J.B.; supervision, Y.C.A. and R.J.B.; project administration, Y.C.A. All authors have read and agreed to the published version of the manuscript.

Funding: This research was supported by Universidad Peruana de Ciencias Aplicadas (UPC) through the UPC-EXPOST-2026-2 program (Internal Funding).

Institutional Review Board Statement: Not applicable.

Informed Consent Statement: Not applicable.

Data Availability Statement: The original contributions presented in this study are included in the article and its Supplementary Materials. Further inquiries may be directed to the corresponding author.

Acknowledgments: The authors gratefully acknowledge the institutional support of the Universidad Peruana de Ciencias Aplicadas.

Conflicts of Interest: The authors declare no conflict of interest.

Abbreviations

The following abbreviations are used in this manuscript:

A	Cooked food
ADM1	Anaerobic Digestion Model No. 1
AI	Antagonism index
BMP	Biochemical methane potential
COD	Chemical oxygen demand

CV	Coefficient of variation
DF	Dark fermentation
DM	Dry matter
DOC	Degradable organic carbon
F	Fruit
GC	Gas chromatography
GWP	Global warming potential
HRT	Hydraulic retention time
LAB	Lactic acid bacteria
LHV	Lower heating value
MCF	Methane correction factor
MSW	Municipal solid waste
PNSB	Purple non-sulfur bacteria
RC	Reference case, 45% *v*/*v* H_2
SB	Stoichiometric bound, 66.7% *v*/*v* H_2
UB	Upper bound, entire gas phase as H_2
UI	Uncertainty interval
V	Vegetables
VFA	Volatile fatty acids
VS	Volatile solids

References

1. Kapdan, I.K.; Kargi, F. Bio-hydrogen production from waste materials. *Enzym. Microb. Technol.* **2006**, *38*, 569–582. [CrossRef]
2. Guo, X.M.; Trably, E.; Latrille, E.; Carrère, H.; Steyer, J.-P. Hydrogen production from agricultural waste by dark fermentation: A review. *Int. J. Hydrogen Energy* **2010**, *35*, 10660–10673. [CrossRef]
3. Ghimire, A.; Frunzo, L.; Pirozzi, F.; Trably, E.; Escudie, R.; Lens, P.N.L.; Esposito, G. A review on dark fermentative biohydrogen production from organic biomass: Process parameters and use of by-products. *Appl. Energy* **2015**, *144*, 73–95. [CrossRef]
4. MINAM. *Sistema de Información para la Gestión de Residuos Sólidos (SIGERSOL): Composición de los Residuos Sólidos Municipales*; Ministerio del Ambiente: Lima, Peru, 2023. Available online: https://sites.google.com/minam.gob.pe/sigersol2/Sigersol-Municipal (accessed on 10 September 2026).
5. CEPLAN. *Observatorio Nacional de Prospectiva: Incremento de los Residuos Sólidos*; Centro Nacional de Planeamiento Estratégico: Lima, Peru, 2025. Available online: https://observatorio.ceplan.gob.pe/ficha/ts_2_amb (accessed on 10 September 2026).
6. Cristóbal, J.; Vázquez-Rowe, I.; Margallo, M.; Ita-Nagy, D.; Ziegler-Rodriguez, K.; Laso, J.; Ruiz-Salmón, I.; Kahhat, R.; Aldaco, R. Climate change mitigation potential of transitioning from open dumpsters in Peru: Evaluation of mitigation strategies in critical dumpsites. *Sci. Total Environ.* **2022**, *846*, 157295. [CrossRef]
7. Hallenbeck, P.C.; Benemann, J.R. Biological hydrogen production; fundamentals and limiting processes. *Int. J. Hydrogen Energy* **2002**, *27*, 1185–1193. [CrossRef]
8. Hawkes, F.R.; Dinsdale, R.; Hawkes, D.L.; Hussy, I. Sustainable fermentative hydrogen production: Challenges for process optimisation. *Int. J. Hydrogen Energy* **2002**, *27*, 1339–1347. [CrossRef]
9. Van Ginkel, S.; Sung, S.; Lay, J.-J. Biohydrogen production as a function of pH and substrate concentration. *Environ. Sci. Technol.* **2001**, *35*, 4726–4730. [CrossRef]
10. Noike, T.; Takabatake, H.; Mizuno, O.; Ohba, M. Inhibition of hydrogen fermentation of organic wastes by lactic acid bacteria. *Int. J. Hydrogen Energy* **2002**, *27*, 1367–1371. [CrossRef]
11. Elbeshbishy, E.; Dhar, B.R.; Nakhla, G.; Lee, H.-S. A critical review on inhibition of dark biohydrogen fermentation. *Renew. Sustain. Energy Rev.* **2017**, *79*, 656–668. [CrossRef]
12. Cabrol, L.; Marone, A.; Tapia-Venegas, E.; Steyer, J.-P.; Ruiz-Filippi, G.; Trably, E. Microbial ecology of fermentative hydrogen producing bioprocesses: Useful insights for driving the ecosystem function. *FEMS Microbiol. Rev.* **2017**, *41*, 158–181. [CrossRef]
13. García-Depraect, O.; Castro-Muñoz, R.; Muñoz, R.; Rene, E.R.; León-Becerril, E.; Valdez-Vazquez, I.; Kumar, G.; Reyes-Alvarado, L.C.; Martínez-Mendoza, L.J.; Carrillo-Reyes, J.; et al. A review on the factors influencing biohydrogen production from lactate: The key to unlocking enhanced dark fermentative processes. *Bioresour. Technol.* **2021**, *324*, 124595. [CrossRef]
14. Detman, A.; Laubitz, D.; Chojnacka, A.; Kiela, P.R.; Salamon, A.; Barberán, A.; Chen, Y.; Yang, F.; Błaszczyk, M.K.; Sikora, A. Dynamics of dark fermentation microbial communities in the light of lactate and butyrate production. *Microbiome* **2021**, *9*, 158. [CrossRef]

15. Redwood, M.D.; Paterson-Beedle, M.; Macaskie, L.E. Integrating dark and light bio-hydrogen production strategies: Towards the hydrogen economy. *Rev. Environ. Sci. Bio/Technol.* **2009**, *8*, 149–185. [CrossRef]
16. Argun, H.; Kargi, F. Bio-hydrogen production by different operational modes of dark and photo-fermentation: An overview. *Int. J. Hydrogen Energy* **2011**, *36*, 7443–7459. [CrossRef]
17. Akkerman, I.; Janssen, M.; Rocha, J.; Wijffels, R.H. Photobiological hydrogen production: Photochemical efficiency and bioreactor design. *Int. J. Hydrogen Energy* **2002**, *27*, 1195–1208. [CrossRef]
18. Adessi, A.; De Philippis, R. Photobioreactor design and illumination systems for H_2 production with anoxygenic photosynthetic bacteria: A review. *Int. J. Hydrogen Energy* **2014**, *39*, 3127–3141. [CrossRef]
19. IPCC. *Good Practice Guidance and Uncertainty Management in National Greenhouse Gas Inventories*; Institute for Global Environmental Strategies: Kanagawa, Japan, 2000.
20. IPCC. *2006 IPCC Guidelines for National Greenhouse Gas Inventories, Volume 5: Waste*; Eggleston, H.S., Buendia, L., Miwa, K., Ngara, T., Tanabe, K., Eds.; Institute for Global Environmental Strategies: Kanagawa, Japan, 2006.
21. Martínez-Mendoza, L.J.; Lebrero, R.; Muñoz, R.; García-Depraect, O. Influence of key operational parameters on biohydrogen production from fruit and vegetable waste via lactate-driven dark fermentation. *Bioresour. Technol.* **2022**, *364*, 128070. [CrossRef]
22. Regueira-Marcos, L.; García-Depraect, O.; Muñoz, R. Elucidating the role of pH and total solids content in the co-production of biohydrogen and carboxylic acids from food waste via lactate-driven dark fermentation. *Fuel* **2023**, *338*, 127238. [CrossRef]
23. Tiegam Tagne, R.F.; Costa, P.; Casella, S.; Favaro, L. Optimization of biohydrogen production by dark fermentation of African food-processing waste streams. *Int. J. Hydrogen Energy* **2024**, *49*, 266–276. [CrossRef]
24. Regueira-Marcos, L.; Muñoz, R.; García-Depraect, O. Continuous lactate-driven dark fermentation of restaurant food waste: Process characterization and new insights on transient feast/famine perturbations. *Bioresour. Technol.* **2023**, *385*, 129385. [CrossRef]
25. Regueira-Marcos, L.; García-Depraect, O.; Muñoz, R. Continuous two-stage lactate-driven dark fermentation process for enhanced biohydrogen production from food waste. *J. Water Process Eng.* **2024**, *67*, 106116. [CrossRef]
26. Noguer, M.C.; Magdalena, J.A.; Bernet, N.; Escudié, R.; Trably, E. Enhanced fermentative hydrogen production from food waste in continuous reactor after butyric acid treatment. *Energies* **2022**, *15*, 4048. [CrossRef]
27. Perat, L.; Escudié, R.; Bernet, N.; Richard, C.; Jégoux, M.; Juge, M.; Trably, E. New insights on waste mixing for enhanced fermentative hydrogen production. *Process Saf. Environ. Prot.* **2024**, *188*, 1326–1337. [CrossRef]
28. Vázquez-López, M.; Moreno-Andrade, I. Biohydrogen production by co-digestion of food waste and corn industry wastewater. *Int. J. Hydrogen Energy* **2025**, *108*, 113–120. [CrossRef]
29. Lee, J.-Y.; Sim, Y.-B.; Jung, J.-H.; Pandey, A.K.; Kyung, D.; Kim, S.-H. Greenhouse gas emissions and net energy production of dark fermentation from food waste followed by anaerobic digestion. *Energy* **2024**, *312*, 133559. [CrossRef]
30. Jin, M.; Wei, X.; Mu, X.; Ren, W.; Zhang, S.; Tang, C.; Cao, W. Life-cycle analysis of biohydrogen production via dark-photo fermentation from wheat straw. *Bioresour. Technol.* **2024**, *396*, 130429. [CrossRef]
31. Zhang, Q.; Jiao, Y.; He, C.; Ruan, R.; Hu, J.; Ren, J.; Toniolo, S.; Jiang, D.; Lu, C.; Li, Y.; et al. Biological fermentation pilot-scale systems and evaluation for commercial viability towards sustainable biohydrogen production. *Nat. Commun.* **2024**, *15*, 4539. [CrossRef]
32. Kim, D.-H.; Kim, S.-H.; Shin, H.-S. Hydrogen fermentation of food waste without inoculum addition. *Enzym. Microb. Technol.* **2009**, *45*, 181–187. [CrossRef]
33. Scheffé, H. Experiments with mixtures. *J. R. Stat. Soc. Ser. B* **1958**, *20*, 344–360. [CrossRef]
34. Cornell, J.A. *Experiments with Mixtures: Designs, Models, and the Analysis of Mixture Data*, 3rd ed.; John Wiley & Sons: New York, NY, USA, 2002.
35. Krause, M.J. Intergovernmental Panel on Climate Change's landfill methane protocol: Reviewing 20 years of application. *Waste Manag. Res.* **2018**, *36*, 827–840. [CrossRef]
36. MINAM. *Guía para la Caracterización de Residuos Sólidos Municipales (Resolución Ministerial N.º 457-2018-MINAM)*; Ministerio del Ambiente: Lima, Peru, 2019. Available online: https://sinia.minam.gob.pe/normas/aprueban-guia-caracterizacion-residuos-solidos-municipales (accessed on 10 September 2026).
37. APHA; AWWA; WEF. *Standard Methods for the Examination of Water and Wastewater*, 23rd ed.; Baird, R.B., Eaton, A.D., Rice, E.W., Eds.; American Public Health Association: Washington, DC, USA, 2017.
38. Dubois, M.; Gilles, K.A.; Hamilton, J.K.; Rebers, P.A.; Smith, F. Colorimetric method for determination of sugars and related substances. *Anal. Chem.* **1956**, *28*, 350–356. [CrossRef]
39. Angelidaki, I.; Alves, M.; Bolzonella, D.; Borzacconi, L.; Campos, J.L.; Guwy, A.J.; Kalyuzhnyi, S.; Jenicek, P.; van Lier, J.B. Defining the biomethane potential (BMP) of solid organic wastes and energy crops: A proposed protocol for batch assays. *Water Sci. Technol.* **2009**, *59*, 927–934. [CrossRef]
40. Holliger, C.; Alves, M.; Andrade, D.; Angelidaki, I.; Astals, S.; Baier, U.; Bougrier, C.; Buffière, P.; Carballa, M.; de Wilde, V.; et al. Towards a standardization of biomethane potential tests. *Water Sci. Technol.* **2016**, *74*, 2515–2522. [CrossRef]

41. Zwietering, M.H.; Jongenburger, I.; Rombouts, F.M.; van 't Riet, K. Modeling of the bacterial growth curve. *Appl. Environ. Microbiol.* **1990**, *56*, 1875–1881. [CrossRef]
42. Welch, B.L. On the comparison of several mean values: An alternative approach. *Biometrika* **1951**, *38*, 330–336. [CrossRef]
43. Games, P.A.; Howell, J.F. Pairwise multiple comparison procedures with unequal *n*'s and/or variances: A Monte Carlo study. *J. Educ. Stat.* **1976**, *1*, 113–125. [CrossRef]
44. Efron, B.; Tibshirani, R.J. *An Introduction to the Bootstrap*; Chapman & Hall: New York, NY, USA, 1993.
45. IPCC. *Climate Change 2021: The Physical Science Basis. Contribution of Working Group I to the Sixth Assessment Report of the Intergovernmental Panel on Climate Change*; Masson-Delmotte, V., Zhai, P., Pirani, A., Connors, S.L., Péan, C., Berger, S., Caud, N., Chen, Y., Goldfarb, L., Gomis, M.I., et al., Eds.; Cambridge University Press: Cambridge, UK; New York, NY, USA, 2021. [CrossRef]
46. Sobol', I.M. Global sensitivity indices for nonlinear mathematical models and their Monte Carlo estimates. *Math. Comput. Simul.* **2001**, *55*, 271–280. [CrossRef]
47. Saltelli, A.; Annoni, P.; Azzini, I.; Campolongo, F.; Ratto, M.; Tarantola, S. Variance based sensitivity analysis of model output. Design and estimator for the total sensitivity index. *Comput. Phys. Commun.* **2010**, *181*, 259–270. [CrossRef]
48. Herman, J.; Usher, W. SALib: An open-source Python library for sensitivity analysis. *J. Open Source Softw.* **2017**, *2*, 97. [CrossRef]
49. Harris, C.R.; Millman, K.J.; van der Walt, S.J.; Gommers, R.; Virtanen, P.; Cournapeau, D.; Wieser, E.; Taylor, J.; Berg, S.; Smith, N.J.; et al. Array programming with NumPy. *Nature* **2020**, *585*, 357–362. [CrossRef]
50. Oliphant, T.E. Python for scientific computing. *Comput. Sci. Eng.* **2007**, *9*, 10–20. [CrossRef]
51. Hunter, J.D. Matplotlib: A 2D graphics environment. *Comput. Sci. Eng.* **2007**, *9*, 90–95. [CrossRef]
52. Wang, K.; Yin, J.; Shen, D.; Li, N. Anaerobic digestion of food waste for volatile fatty acids (VFAs) production with different types of inoculum: Effect of pH. *Bioresour. Technol.* **2014**, *161*, 395–401. [CrossRef]
53. Roslan, E.; Magdalena, J.A.; Mohamed, H.; Akhiar, A.; Shamsuddin, A.H.; Carrere, H.; Trably, E. Lactic acid fermentation of food waste as storage method prior to biohydrogen production: Effect of storage temperature on biohydrogen potential and microbial communities. *Bioresour. Technol.* **2023**, *378*, 128985. [CrossRef]
54. Villanueva-Galindo, E.; Pérez-Rangel, M.; Moreno-Andrade, I. Evaluation of individual and combined effect of lactic acid-consuming bacteria on mesophilic hydrogen production from lactic acid effluent from food waste treatment. *Bioresour. Technol.* **2024**, *408*, 131224. [CrossRef]
55. Martínez-Fraile, C.; Muñoz, R.; Simorte, M.T.; Sanz, I.; García-Depraect, O. Biohydrogen production by lactate-driven dark fermentation of real organic wastes derived from solid waste treatment plants. *Bioresour. Technol.* **2024**, *403*, 130846. [CrossRef]
56. Moreno-Andrade, I.; Berrocal-Bravo, M.J.; Valdez-Vazquez, I. Biohydrogen production from food waste and waste activated sludge in codigestion: Influence of organic loading rate and changes in microbial community. *J. Chem. Technol. Biotechnol.* **2023**, *98*, 230–237. [CrossRef]
57. Kim, G.; Cho, K.-S. Bacterial synergy and relay for thermophilic hydrogen production through dark fermentation using food waste. *Bioresour. Technol.* **2025**, *416*, 131748. [CrossRef]
58. Das, S.R.; Basak, N. Enhancing biohydrogen production by optimization of waste potato concentration in dark and photo fermentation. *J. Clean. Prod.* **2025**, *494*, 145000. [CrossRef]
59. Gbiete, D.; Brügging, E.; Narra, S.; Kongnine, D.M. Comprehensive characterization and assessment of biohydrogen production potential of restaurant food waste for scalable dark fermentation systems. *Biomass Bioenergy* **2026**, *204*, 108444. [CrossRef]
60. Batstone, D.J.; Keller, J.; Angelidaki, I.; Kalyuzhnyi, S.V.; Pavlostathis, S.G.; Rozzi, A.; Sanders, W.T.M.; Siegrist, H.; Vavilin, V.A. The IWA Anaerobic Digestion Model No 1 (ADM1). *Water Sci. Technol.* **2002**, *45*, 65–73. [CrossRef]
61. Penumathsa, B.K.V.; Premier, G.C.; Kyazze, G.; Dinsdale, R.; Guwy, A.J.; Esteves, S.; Rodríguez, J. ADM1 can be applied to continuous bio-hydrogen production using a variable stoichiometry approach. *Water Res.* **2008**, *42*, 4379–4385. Erratum in *Water Res.* **2009**, *43*, 562. . [CrossRef]
62. Gadhamshetty, V.; Arudchelvam, Y.; Nirmalakhandan, N.; Johnson, D.C. Modeling dark fermentation for biohydrogen production: ADM1-based model vs. Gompertz model. *Int. J. Hydrogen Energy* **2010**, *35*, 479–490. [CrossRef]

Disclaimer/Publisher's Note: The statements, opinions and data contained in all publications are solely those of the individual author(s) and contributor(s) and not of MDPI and/or the editor(s). MDPI and/or the editor(s) disclaim responsibility for any injury to people or property resulting from any ideas, methods, instructions or products referred to in the content.